Subsurface fluid flow in the deep-water Kwanza Basin, offshore Angola

Christophe Serié,* Mads Huuse,† Niels H. Schødt,‡ James M. Brooks§ and Alan Williams¶

*Global New Ventures Exploration, ConocoPhillips Company, Houston, TX, USA
†Basin Studies and Petroleum Geoscience Research Group, SEAES, University of Manchester, Manchester, UK
‡Exploration Department, Maersk Oil, Copenhagen K, Denmark
§TDI-Brooks International, College Station, TX, USA
¶CGG NPA Ltd, Edenbridge, Kent, UK

ABSTRACT

Integrated analysis of high-quality three-dimensional (3D) seismic, seabed geochemistry, and satellite-based surface slick data from the deep-water Kwanza Basin documents the widespread occurrence of past and present fluid flow associated with dewatering processes and hydrocarbon migration. Seismic scale fluid flow phenomena are defined by seep-related seafloor features including pockmarks, mud or asphalt volcanoes, gas hydrate pingoes, as well as shallow subsurface features such as palaeo-pockmarks, direct hydrocarbon indicators (DHIs), pipes and bottom-simulating reflections (BSRs). BSR-derived shallow geothermal gradients show elevated temperatures attributed to fluid advection along inclined stratigraphic carrier beds around salt structures in addition to elevated shallow thermal anomalies above highly conductive salt bodies. Seabed evidences of migrated thermogenic hydrocarbons and surface slicks are used to differentiate thermogenic hydrocarbon migration from fluid flow processes such as dewatering and biogenic gas migration. The analysis constrains the fluid plumbing system defined by the three-dimensional distribution of stratigraphic carriers and seal bypass systems through time. Detailed integration and iterative interpretation have confirmed the presence of mature source rock and effective migration pathways with significant implications for petroleum prospectivity in the post-salt interval. Integration of seismic, seabed geochemistry and satellite data represents a robust method to document and interpret fluid flow phenomena along continental margins, and highlights the importance of integrated fluid flow studies with regard to petroleum exploration, submarine geohazards, marine ecosystems and climate change.

INTRODUCTION

Past and present fluid flow phenomena along continental margins reflect the dynamic evolution of sedimentary basins with numerous implications for energy resources, marine ecosystems, submarine geohazards and climate change (Milkov & Sassen, 2002; Sultan *et al.*, 2004; Berndt, 2005; Cartwright, 2007; Judd & Hovland, 2007; Huuse *et al.*, 2010; Maslin *et al.*, 2010; Anka *et al.*, 2012). Understanding subsurface fluid flow processes has recently been a major area of interest in petroleum exploration following a growing demand for energy and associated shift towards challenging exploration settings along deep-water continental margins (White *et al.*, 2003). Recent advances in seismic imaging have greatly enhanced the detailed observation, mapping and inter-

pretation of shallow fluid flow phenomena over large areas (Cowley & O'Brien, 2000; Van Rensbergen *et al.*, 2003; Lucazeau *et al.*, 2004; Ligtenberg, 2005; Cartwright *et al.*, 2007; Løseth *et al.*, 2009; Huuse *et al.*, 2010). Seafloor fluid flow features and associated overburden anomalies have helped to define the nature, timing and intensity of fluid migration in relation to depositional, structural and diagenetic processes including hydrocarbon generation, migration and seepage. However, direct calibration with seabed geochemistry and satellite-based surface slick are limited to a handful of studies (Abrams, 1992; Hood *et al.*, 2002; Williams & Lawrence, 2002; O'Brien *et al.*, 2005; Garcia-Pineda *et al.*, 2010; Logan *et al.*, 2010).

This paper presents the first integrated fluid flow study in the deep-water Kwanza Basin based on high-quality three-dimensional (3D) seismic, seabed geochemistry and satellite-based surface slick data. Detailed seismic interpretation shows the presence of numerous fluid flow phenomena including seep-related seafloor features, overburden seismic anomalies and associated plumbing

Correspondence: Christophe Serié, Global New Ventures Exploration, ConocoPhillips Company, 600 North Dairy Ashford, Houston, TX 77079, USA. E-mail: christophe.serie@conocophillips.com

systems. Direct comparison with surface geochemistry and satellite-based surface slick data is used to confirm the presence of seismically well-defined seeps and validate ambiguous seep-related features. Seabed geochemistry was also used to determine the origin of migrated thermogenic hydrocarbons and confirm potential migration pathways along networks of stratigraphic carriers and seal bypass systems. Shallow geothermal gradients derived from BSR modelling suggest relative contributions from enhanced conduction through salt and advection from fluid migration. Finally, the importance of integrated studies and iterative interpretation is discussed with regard to fluid flow processes and petroleum exploration in frontier sedimentary basins.

GEOLOGICAL SETTING

The Angolan continental margin is known as a world-class petroleum province comprising a series of sedimentary basins (Katz & Mello, 2000), including the Lower Congo, Kwanza, Benguela and Namibe basins formed as a result of Late Jurassic to Early Cretaceous breakup of Gondwana and subsequent opening of the South Atlantic Ocean (Guiraud & Maurin, 1992; Karner & Driscoll, 1999; Fig. 1). The tectono-stratigraphic evolution of the Kwanza Basin resulted in three major sequences: pre-salt (Late Proterozoic–Barremian), salt (Aptian) and post-salt (Albian–Holocene) (Ala & Selley, 1997; Schollnberger, 2001), all of which comprise key elements of the Angolan petroleum systems (Danforth, 1997; Brownfield & Charpentier, 2006; Beglinger *et al.*, 2012; Fig. 2). The pre-salt sequence is defined by a series of intracratonic basins dominated by continental deposits (Brice *et al.*, 1982). Following the continental break-up, initial rifting formed a series of lacustrine basins within structural troughs trending parallel to the present-day coastline and dominated by siliciclastic and carbonate deposits (Uncini *et al.*, 1998). The principal source rock for the pre-salt sequence consists of the regionally extensive and prolific Cuvo lacustrine shale associated with hydrocarbon accumulations within the Grey Cuvo sandstones and lacustrine Toca carbonates (Danforth, 1997; Uncini *et al.*, 1998; Burwood, 1999). The onset of restricted marine conditions led to the deposition of thick evaporites that facilitated later gravity-driven thin-skinned deformation of the post-salt sequence. Regionally, the post-salt sequence is characterized by an upper slope extensional domain with grabens and rafts, as well as a downslope contractional domain dominated by salt diapirs, salt walls and salt nappes (Duval *et al.*, 1992; Lundin, 1992; Marton *et al.*, 2000; von Nicolai, 2011; Quirk *et al.*, 2012). In addition to structural deformation and subsequent trap formation in the post-salt interval, the Loeme salt (Aptian) represents a regional and effective seal for the pre-salt sequence (Danforth, 1997; Brownfield & Charpentier, 2006), apart from locations where salt welds allow pre-salt oil migration into post-salt reservoirs (Danforth, 1997). The post-

salt sedimentary succession is marked by an initial rapid marine transgression dominated by the development of carbonate platforms (Albian) followed by open marine conditions characterized by clastic progradation and deep-water sedimentation (Cenomanian–Oligocene) (Schollnberger, 2001; Goldhammer *et al.*, 2002). Subsequent tectonic uplift coupled with eustatic lowering resulted in erosion on the shelf and downslope deposition of turbidite fan systems within salt minibasins (Lunde *et al.*, 1992; Jackson *et al.*, 2005; Hay, 2012). Pliocene to present-day is dominated by hemipelagic silts and clays apart from coarser sediments associated with channels and fan lobes constrained to river entry points (Pufahl *et al.*, 1998). The post salt interval presents numerous organic-rich source rock intervals (Binga, Itombe, N'Golome, Teba, Rio Dande, Cunga fms.) (Danforth, 1997; Burwood, 1999; Hartwig *et al.*, 2012) and reservoirs ranging from Albian shelf carbonates to Tertiary deep-water fans (Danforth, 1997; Brownfield & Charpentier, 2006). The Pliocene to Holocene succession, along with the predominant mudstone intervals of the Oligocene–Miocene succession, are therefore commonly considered as competent seals for the prolific Oligocene-Miocene turbidite reservoirs (Brownfield & Charpentier, 2006).

DATABASE

This study is primarily based on a high-quality, prestack time-migrated, three-dimensional (3D) seismic volume acquired in 2009 by Maersk Oil, in addition to regional two-dimensional (2D) seismic lines and 12 exploration wells (Fig. 3). The 3D volume covers an area of 3000 km^2 in water depths ranging from 640 m to 1630 m with a line spacing of 12.5 m and sampling interval of 4 ms two-way traveltime (TWT). The studied interval is imaged with a dominant frequency of 40 Hz, which gives a vertical resolution ($\lambda/4$) of $\sim$ 11–16 m and horizontal resolution ($\lambda/2$) of $\sim$ 22–31 m, assuming seismic velocities between 1800 m/s and 2500 m/s (Sheriff, 1985). The seismic data are zero phase with a positive amplitude representing a downward increase in acoustic impedance depicted by a red, orange or yellow peak. Negative amplitudes represent downward decreasing acoustic impedance and are depicted by a light blue trough. The focus of this study has been the post-salt interval down to 4 s TWT due to restricted access to seismic data from the pre-salt interval.

The seabed geochemistry data consists of 55 piston cores analysed by TDI-Brooks International. All piston core locations were selected based on regional 2D seismic lines during a number of sampling campaigns between 1984 and 1996. The database includes a full set of geochemical analyses including Total Scanning Fluorescence (TSF), Headspace Gas Analysis (HS), C15+ Hydrocarbon Analysis, as well as piston core descriptions (Fig. 3).
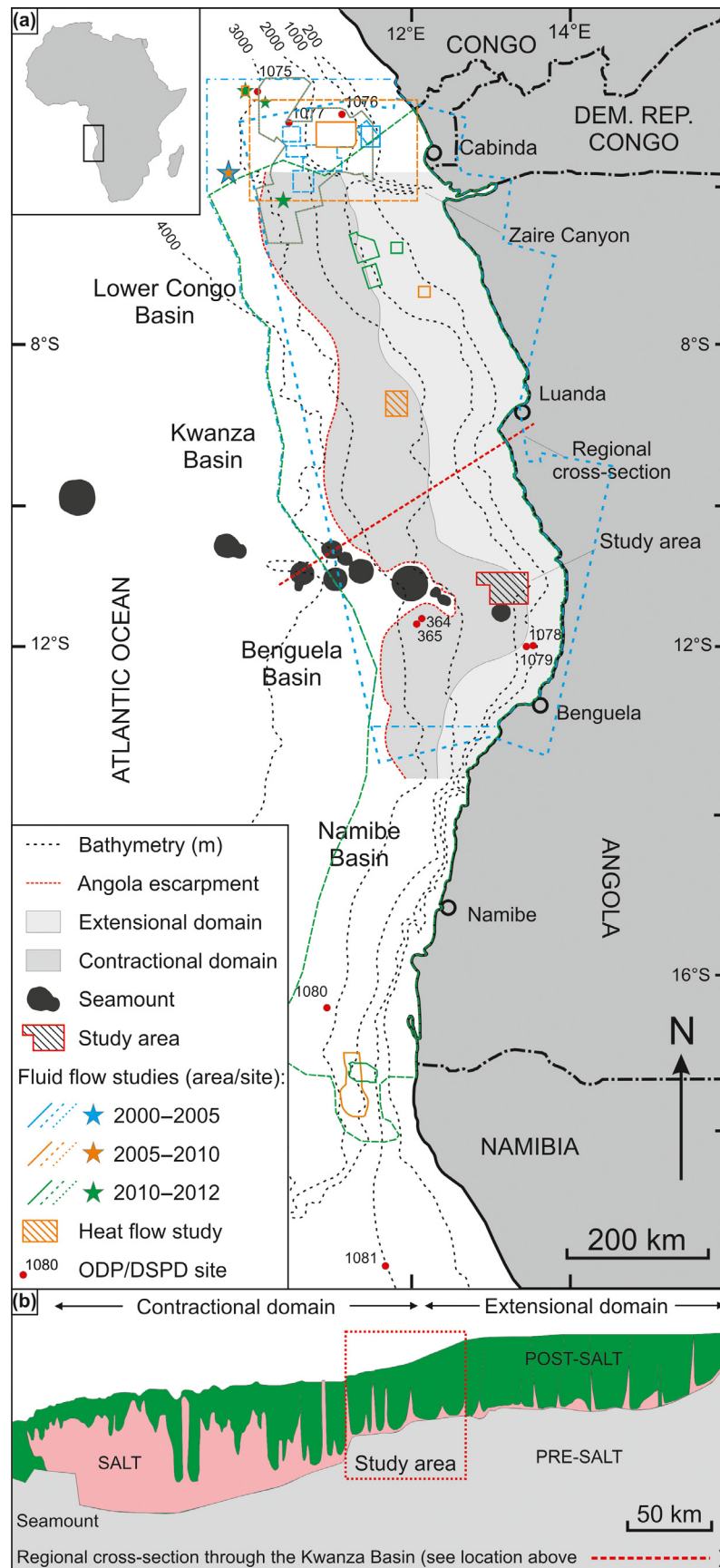
Fig. 1. (a) Simplified tectonic map of the Angolan continental margin including main sub-basins, major tectonic elements (Marton *et al.*, 2000) and historical review of fluid flow studies (Serié, 2013). (b) Geological cross-section illustrating the regional tectono-strati-graphic framework through the Kwanza Basin (Marton *et al.*, 2000; Quirk *et al.*, 2012).
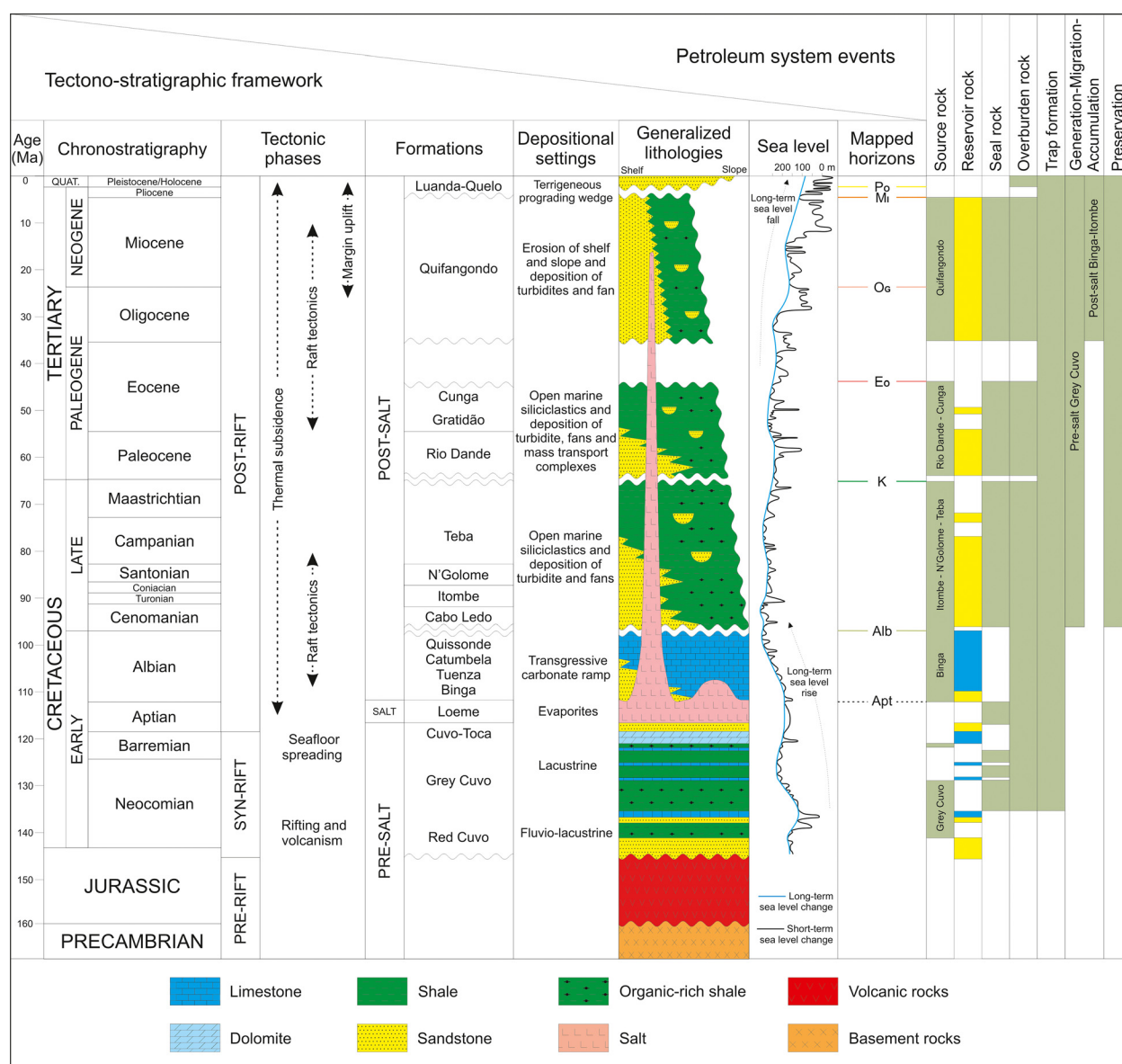
Fig. 2. Kwanza Basin chrono–stratigraphic chart summarizing tectono–stratigraphic framework and petroleum system events (Brice *et al.*, 1982; Haq *et al.*, 1987; Duval *et al.*, 1992; Guiraud & Maurin, 1992; Lunde *et al.*, 1992; Lundin, 1992; Ala & Selley, 1997; Danforth, 1997; Pufahl *et al.*, 1998; Uncini *et al.*, 1998; Burwood, 1999; Karner & Driscoll, 1999; Marton *et al.*, 2000; Schollnberger, 2001; Goldhammer *et al.*, 2002; Jackson *et al.*, 2005; Brownfield & Charpentier, 2006; von Nicolai, 2011; Beglinger *et al.*, 2012; Hay, 2012; Quirk *et al.*, 2012).

Satellite–based surface slick interpretations provided by Fugro NPA form part of a regional study based on 15 synthetic–aperture radar (SAR) scenes in the Kwanza Basin, and include 12 SAR scenes over the study area (Fig. 3). Seep interpretation includes slick emission points, slick outlines, clustered slicks and slick categories.

METHODOLOGY

3D seismic

The tectono–stratigraphic framework within the study area is interpreted using standard seismic stratigraphic techniques based on reflection terminations and seismic facies (Mitchum *et al.*, 1977). The post–salt sequence is divided into chronostratigraphic intervals based on existing regional seismic interpretations calibrated to nearby exploration wells (Fig. 3a) (Schollnberger, 2001; Hudec & Jackson, 2004; von Nicolai, 2011), including data from a recent exploration well drilled within the study area (Maersk pers. comm., 2012). In addition to the standard seismic stratigraphic techniques, structural interpretation mainly linked with salt tectonics is defined using seismic facies, variance attributes and geometrical comparison with known salt–related structures including salt diapirs, salt walls, salt nappes and associated structural deformation (Alsop, 1996; Hudec & Jackson, 2007; Dooley *et al.*, 2012). Detailed interpretation of chronostratigraphic
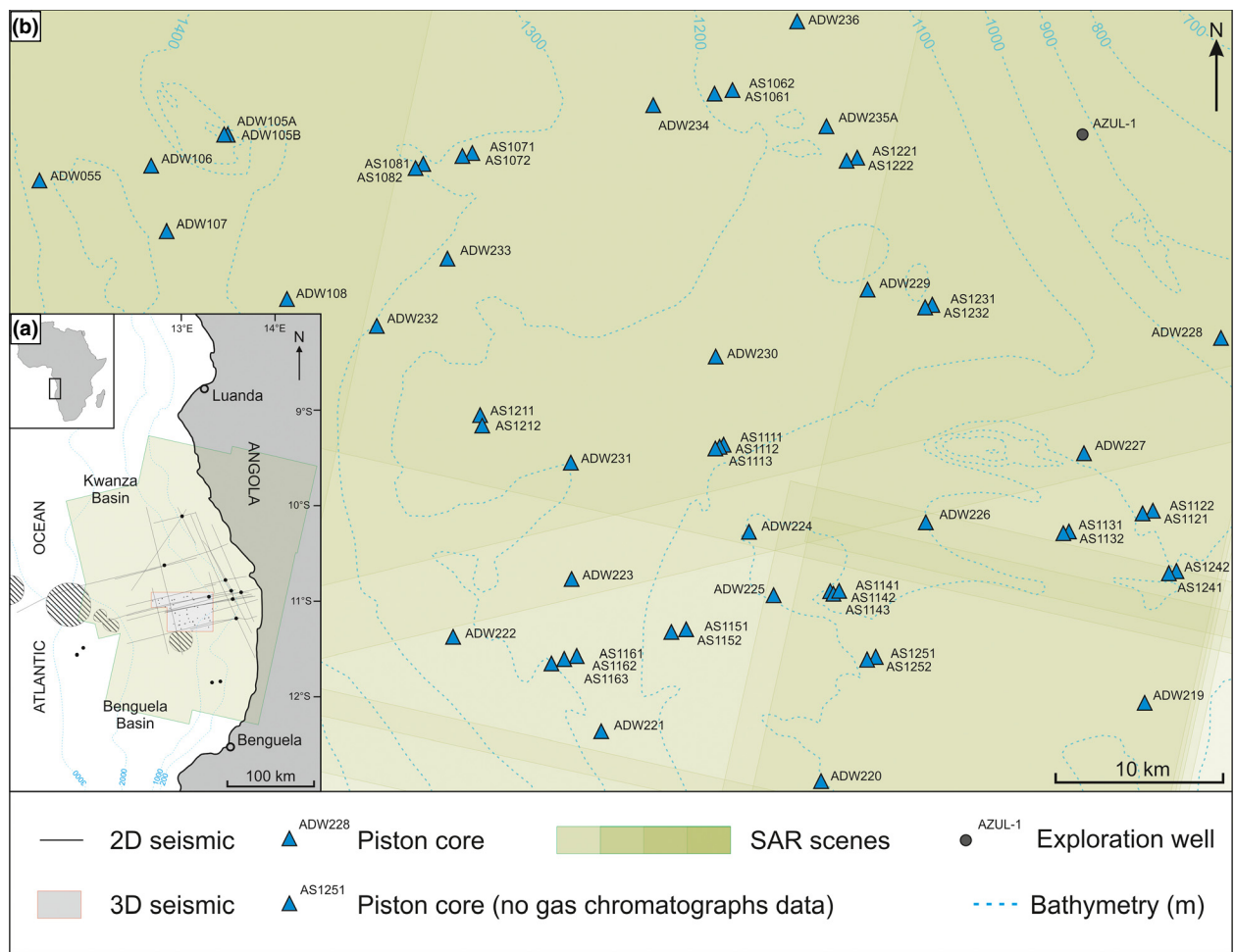
Fig. 3. (a) Map of the Kwanza Basin along the Angolan continental margin showing the location of the study area and extent of available data including regional two-dimensional (2D) seismic lines, three-dimensional (3D) seismic volume, exploration wells, satellite seep data and seabed geochemical survey. (b) Map of the study area with available data including 3D seismic volume covering 3000 km^2, 55 pistons cores solely selected on regional 2D seismic lines and 12 synthetic-aperture radar (SAR) scenes.

intervals was used to create a seafloor geological map highlighting the distribution and extent of exposed stratigraphic intervals at the present day seafloor.

Seismic scale fluid flow phenomena are defined by the occurrence of seep-related features on the seafloor and associated seismic anomalies in the shallow subsurface. The bathymetry within the study area is derived from time-depth conversion of the interpreted seafloor TWT-structure map and assuming a seawater velocity of 1500 m/s. Detailed observations and interpretations of seep-related fluid flow features were fine-tuned using seafloor seismic reflectivity, discontinuity and dip attributes characterizing both morphological and geophysical signatures of particular fluid flow features such as pockmarks, mud volcanoes, mud mounds, gas hydrate pingoes, carbonate mounds and possible asphalt volcanoes (Roberts, 2001; Roberts *et al.*, 2006; Evans *et al.*, 2007; Judd & Hovland, 2007; Jones *et al.*, 2014). Negative amplitude anomalies are interpreted as the result of free gas in surface sediments or unconsolidated gas bearing sediment extrusions (Evans *et al.*, 2007), as opposed to positive amplitude anomalies generally asso-

ciated with the occurrence of denser sediments, hard-grounds, precipitated authigenic carbonates, layer of shell debris or surface gas hydrates (Roberts, 2001; Judd & Hovland, 2007).

Overburden seismic anomalies are defined by detailed mapping of reflection amplitudes, shapes and spatial distribution. The occurrence of past and present fluid flow is characterized by the presence of direct hydrocarbon indicators (DHIs), bottom-simulating reflections (BSRs), hydrocarbon-related diagenetic zones (HRDZs), pipes, polygonal faults, diagenetic fronts, sediment injections and volcanic intrusions (Shipley *et al.*, 1979; Løseth *et al.*, 2009; Huuse *et al.*, 2010). Bottom-simulating reflections (BSRs) are usually considered as the seismic expression of free gas below hydrate-bearing sediment (Singh *et al.*, 1993; Berndt *et al.*, 2004). BSRs are commonly characterized by a strong, reversed-polarity reflection generally following the seafloor topography and occasionally crosscutting stratal reflections in areas of complex structure (Shipley *et al.*, 1979). Recent advances in three-dimensional seismic imaging have revealed the common occurrence of more subtle and complex BSR

types including discontinuous and pluming BSRs (Shedd *et al.*, 2012).

Seabed geochemistry

Seabed geochemistry analyses are based on sediment samples from piston cores up to 6 m in length with location selected on regional 2D seismic lines, or where available on 3D seismic and swath bathymetry data. Three sediment sections near the bottom of the core are generally sampled to determine near-surface indication of migrated thermogenic hydrocarbons by measuring Total Scanning Fluorescence (TSF) intensities of sediment extracts, light hydrocarbons by headspace extraction and C_{15+} hydrocarbons by gas chromatography in sediment extracts (Abrams, 2013). TSF detects and measures organic compounds containing one or more aromatic rings; increasing TSF intensity corresponds to increasing amount of aromatic compounds in sediment extract characterizing the presence of migrated thermogenic hydrocarbon in near surface sediments (Abrams, 2005). Headspace Gas Analysis determines the concentration of light hydrocarbon gases including methane, ethane, propene, propane, butenes, iso-butane, n-butane, neopentane, iso-pentane and n-pentane. Light hydrocarbons are used to evaluate anomalous hydrocarbon sources (bacterial vs. thermogenic) (Brooks *et al.*, 1983; Abrams, 1992). C15+ Hydrocarbon analysis determines the concentration of high molecular weight hydrocarbons (C_{15+}) based on sediment extract gas chromatography. C_{15+} analysis provide gas chromatograms and C_{15} to C_{34} n-alkane, pristane, phytane and unresolved complex mixture (UCM) concentrations for sediment extracts in order to evaluate the presence of migrated thermogenic hydrocarbons (Abrams, 1992).

Satellite-based surface slicks

Surface slick distribution and intensity are interpreted from satellite-based remote sensing data. Synthetic Aperture Radar (SAR) has proven to be highly successful in delineating natural hydrocarbon seepages from oil slicks on the sea surface (Garcia-Pineda *et al.*, 2010; Logan *et al.*, 2010). SAR sensors send out a microwave signal, typically with a wavelength of several centimetres and build an image from the radiation reflected back to the satellite (Lawrence *et al.*, 1998). SAR slicks are areas that have anomalously low backscatter values compared to background level as a result of dampened capillary waves on the ocean surface. Dampening of the capillary waves may occur through a variety of causes which include natural film slicks, pollution slicks and seepage slicks. Seep origins are defined based on parameters such as size, location, morphology, flow direction, repetition, edge characteristics, ocean features and geological context (Lawrence *et al.*, 1998; Williams & Lawrence, 2002). Slick occurrences are also controlled by the type of leaking hydrocarbons and commonly associated with oil, as opposed to gas

and very light oil that quickly disperse and evaporate. The horizontal displacement of surface slicks from its seafloor vents will depend on the water column and surface currents where seeps can be found in a circumference of up to five times the water depth, and occasionally up to tens of kilometres due to the horizontal layering of the sea (Garcia-Pineda *et al.*, 2010).

BSR-derived shallow geothermal gradient

Commonly observed along the continental slopes, BSRs are generally associated with the base of the gas hydrate stability zone (GHSZ) defining the subsurface depth below which natural gas hydrates are no longer stable (Sloan & Koh, 2008). Based on natural gas hydrate stability conditions, water bottom temperature and thermal conductivity, BSR depths can be used to estimate shallow geothermal gradients and associated surface heat flow (Yamano *et al.*, 1982; Grevemeyer & Villinger, 2001). In addition to the conventional surface heat flow measurements and with relatively good consistency (Lucazeau *et al.*, 2004), this approach has been applied to both single reflection profiles and three-dimensional reflection data sets. Widespread BSRs are used to estimate shallow geothermal gradient over large areas while providing significant constraints to understanding processes along continental margin scale such as local thermal anomalies associated with fluid flow (Grevemeyer *et al.*, 2004; Hornbach *et al.*, 2012), contrasts in thermal conductivity between sedimentary formations (Lucazeau *et al.*, 2004) and surface processes including erosion and sedimentation (Martin *et al.*, 2004).

Bottom-simulating reflection-derived shallow geothermal gradient estimations correspond to the temperature difference between bottom-water temperature at the seafloor and estimated temperature at BSR-depth. Bottom-water temperatures of the Kwanza Basin (between latitudes 8°S to 12°S and longitudes 10°E to 14°E) were derived from seawater temperature data compiled from the NOAA-NODC World Ocean Atlas (Locarnini *et al.*, 2010). Temperatures at BSR-depth were estimated from empirical gas hydrate stability law for seawater salinity and methane system (Lu & Sultan, 2008):

$$P(T, S) = \exp((Cs.S + Ds).T). \exp(Es.S).Fs,$$

where (P is hydrostatic pressure in kPa, T is temperature at the base of the GHSZ in K, S is salinity in pore water ($0 < S \leq 0.050$ mol NaCl/mol H_2O) and coefficients Cs = 0.1711726397, Ds = 0.1046133676, Es = -34.14836102 and Fs = $1.010769956 \times 10^{-9}$).

Pressure at BSR depths are based on hydrostatic pressure encompassing water column height and BSR thickness. BSR thicknesses are determined from time-depth conversion using seismic velocity analysis with velocity ranging between 1500 and 2400 m/s due to lateral variability within sedimentary rock outcropping at the seafloor. In the absence of fluid composition data, a simple seawater salinity-pure methane system was used while
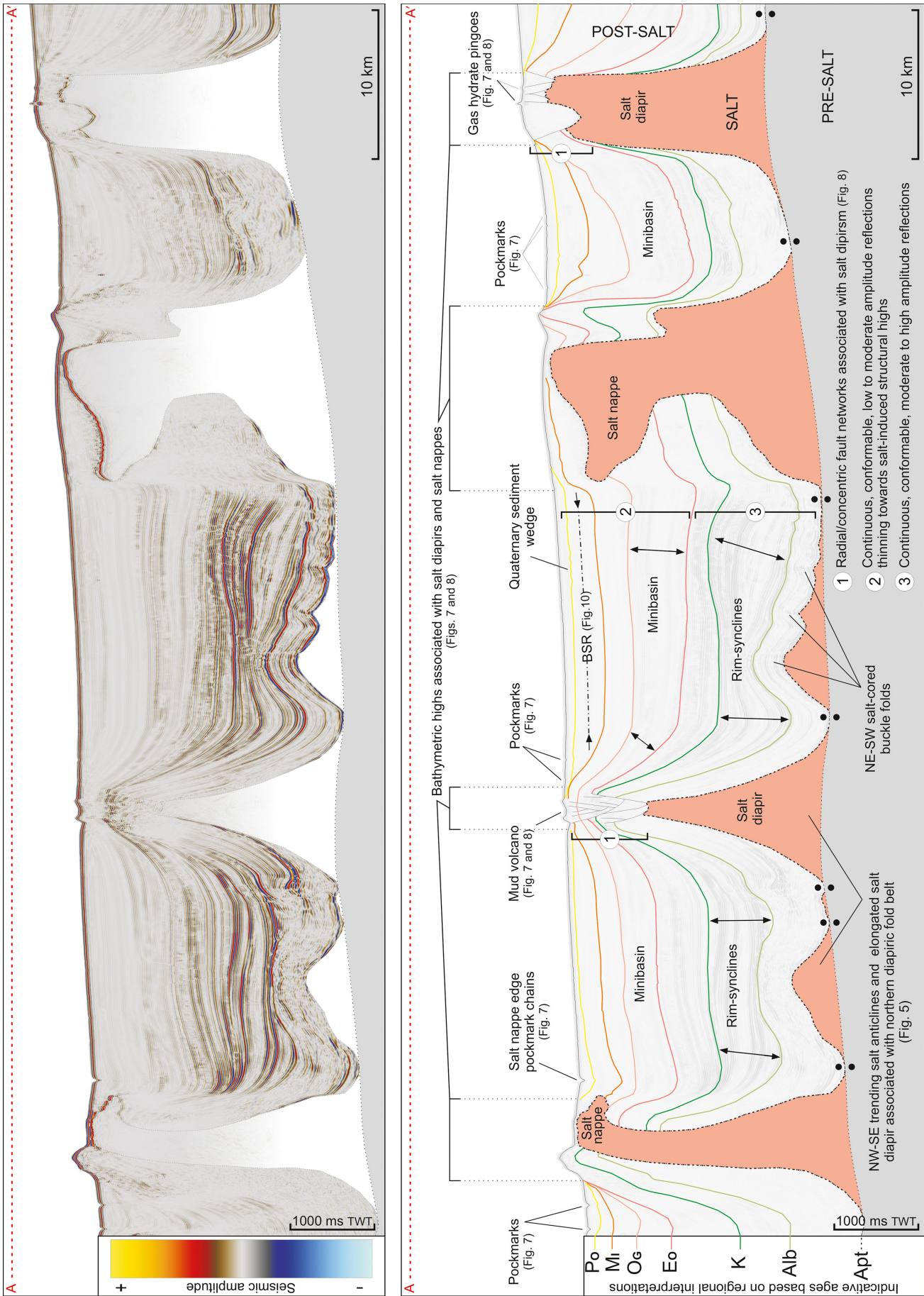
Fig. 4. Two-dimensional seismic profile A–A' illustrating the present-day basin configuration and associated tectono–stratigraphic evolution mainly controlled by salt tectonics with the development of salt diapir (sd), salt nappe (sn) and minibasin (mb). Note the presence of broad bathymetric highs over salt-related structure and seep-related seafloor features above salt diapir (see Figs 5, 7, and 8).
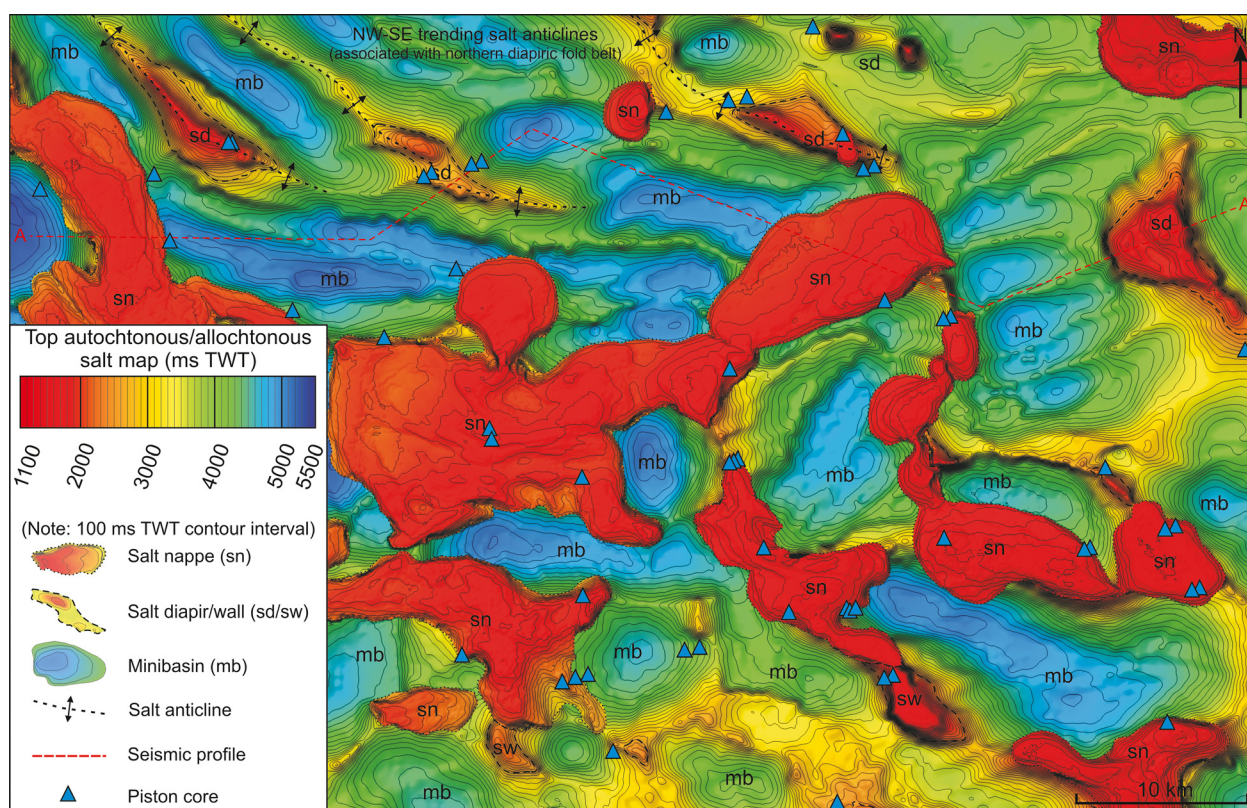
Fig. 5. Post-salt isochron map (ms TWT) highlighting post-salt basin geometry with the presence of minibasin (mb), salt diapir (sd), salt nappe (sn), salt wall (sw) and regional structural elements.
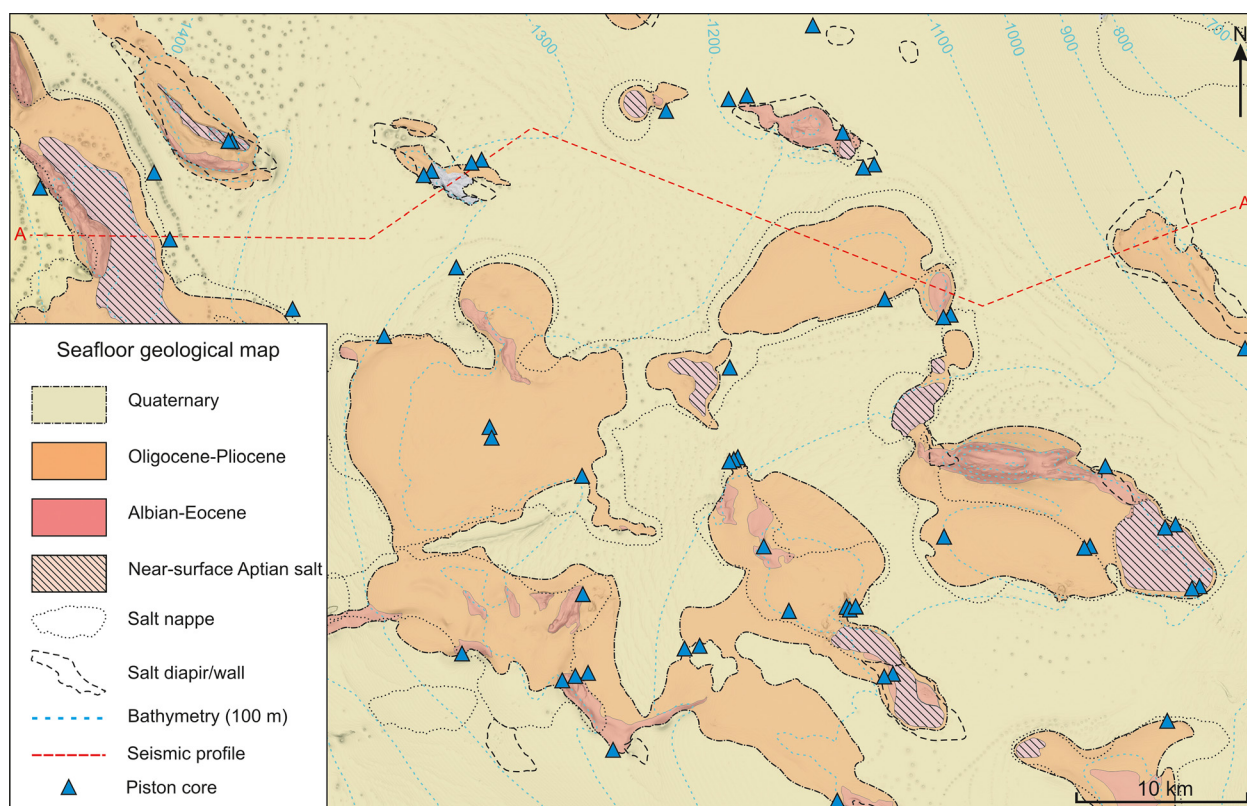

Fig. 6. Seafloor geological map highlighting the distribution of outcropping stratigraphic units (Aptian–Eocene, Eocene–Pliocene, Quaternary) as a result of structural deformation associated with intense salt tectonics.

considering uncertainty associated with fluid composition and pore fluid salinity (Holder *et al.*, 1987; Dickens & Quinby–Hunt, 1994; Sloan & Koh, 2008; Minshull & Keddie, 2010).

RESULTS

3D seismic

Tectono-stratigraphic framework

Three-dimensional seismic interpretation based on the regional tectono-stratigraphic framework indicates the presence of a thick (>5500 ms TWT) post-salt interval strongly affected by salt tectonics (Figs 4 and 5). The base of the post-salt interval is defined by the top salt reflection characterized by a strong positive amplitude in the shallow section, as opposed to a negative amplitude in the deeper section due to overlying Albian carbonates with relatively higher velocity and density compared to underlying salt (Fig. 4). The salt is characterized by reflection-free to chaotic reflections defining the presence of numerous salt related structures including salt diapirs, salt walls and salt nappes (Figs 4 and 5). The present-day structural framework is dominated by salt-cored anticlines trending NW-SE and associated elongated salt diapirs to the north, as opposed to salt walls and salt nappes to the south (Fig. 5). In a regional context, the occurrence of NW-SE trending salt-cored anticlines is linked to the more extensive diapiric fold belt documented to the north (Marton *et al.*, 2000; von Nicolai, 2011). In addition to Tertiary salt tectonics, the Albian interval is characterized by the presence of NE–SW-oriented buckle folds and thrusts interpreted to represent an early phase of syn-sedimentary salt deformation and comprises divergent stratigraphic intervals related to the development of rim-synclines linked to early salt diapirism during the Late Cretaceous (Quirk *et al.*, 2012). Present-day seafloor is characterized by the presence of broad bathymetric highs representing the surface expression of underlying salt structures, and generally associated with older stratigraphic units outcropping at the seafloor (Fig. 6).

The post-salt interval has been subdivided into seven seismic-statigraphic units bounded by eight interpreted seismic horizons tied to the regional stratigraphic framework (Fig. 4). The Albian interval is defined by continuous, conformable, moderate to high amplitude reflections and commonly affected by NE–SW-oriented salt-cored buckle folds. The Cretaceous interval is defined by divergent stratigraphic intervals, development of rim-syclines. The Eocene–Oligocene interval is characterized by low to moderate amplitude reflections showing overall thinning toward salt-induced structural highs and characterized by the predominance of Oligocene mass transport deposits (MTDs). The MTDs are generally associated with salt remobilization and subsequent instability above salt diapir

flanks and redeposition within minibasins. The Miocene–Pliocene section is defined by continuous, conformable, moderate to high amplitude reflections, as opposed to numerous fan/channel complexes observed in the northern part of the Kwanza Basin (Hay, 2012) as well as highly polygonally faulted interval documented in the Lower Congo Basin (Gay *et al.*, 2004; Andresen & Huuse, 2011). Nonetheless, the Miocene–Pliocene section is characterized by the presence of bowl-shaped structures up to 300 ms TWT in depth and 4 km in diameter (Fig. 7). Bowl-shaped features are interpreted as time-transgressive bedforms formed by bottom current scour around bathymetric highs (Serié, 2013), however, features with similar size have also been interpreted as funnel-shaped collapse linked to gas hydrate dissociation (Ho *et al.*, 2012; Imbert & Ho, 2012). The Quaternary section is defined by moderate to high amplitude reflections associated with the presence of a deep-water fan complex originating from the southeast corner of the study area (Fig. 7).

Seafloor fluid flow phenomena

Detailed 3D seismic interpretation reveals a wide variety of fluid flow-related features on the seafloor including pockmarks and mounds of variable sizes and rugosities (Figs 7 and 8). The seafloor dip map highlights the presence of pockmarks with varying degree of intensity with randomly distributed pockmarks in minibasins, curvilinear pockmark trends following the edge of salt nappes, pockmarks along fault scarps, linear pockmark trends following the axes of Quaternary minibasin depocentres, pockmarks controlled by seabed sediments and the presence of bowl-shaped structures (Fig. 7). In addition to the predominant occurrence of pockmarks, distinct mounded features above topographic highs are also documented based on dip attribute and seismic reflectivity seafloor maps (Figs 7 and 8). Figure 8b shows the presence of protruding features defined by circular to ellipsoidal mounds of 80–300 m in extent and 5–40 m in height. Mound morphologies vary from smooth, well-rounded, steep-sided mounds (9°–16°) (M1, M2, M6) to rough, uneven, gently dipping mounds (3°–10°) (M4, M5, M7, M8). The mounds are characterized by higher reflectivity than the seafloor, indeed appearing as high amplitude anomalies. Detailed interpretation suggests that the occurrence of these mounds is most likely related to the development of gas hydrate pingoes associated with the formation and dissociation of massive gas hydrate in the shallow subsurface (Serié *et al.*, 2012). Figure 8d shows the presence of another protruding feature defined by a circular central apex about 0.5 km in diameter and up to 50 m in height, and elongated branches of 1.5–2.5 km in extent with height up to 25 m trending along faults bounding the crestal collapse of the underlying salt diapir. Away from the central apex, one of the elongated branches lines-up directly with a fault scarp bordered by a series of individual pockmarks (Fig. 8d). This feature
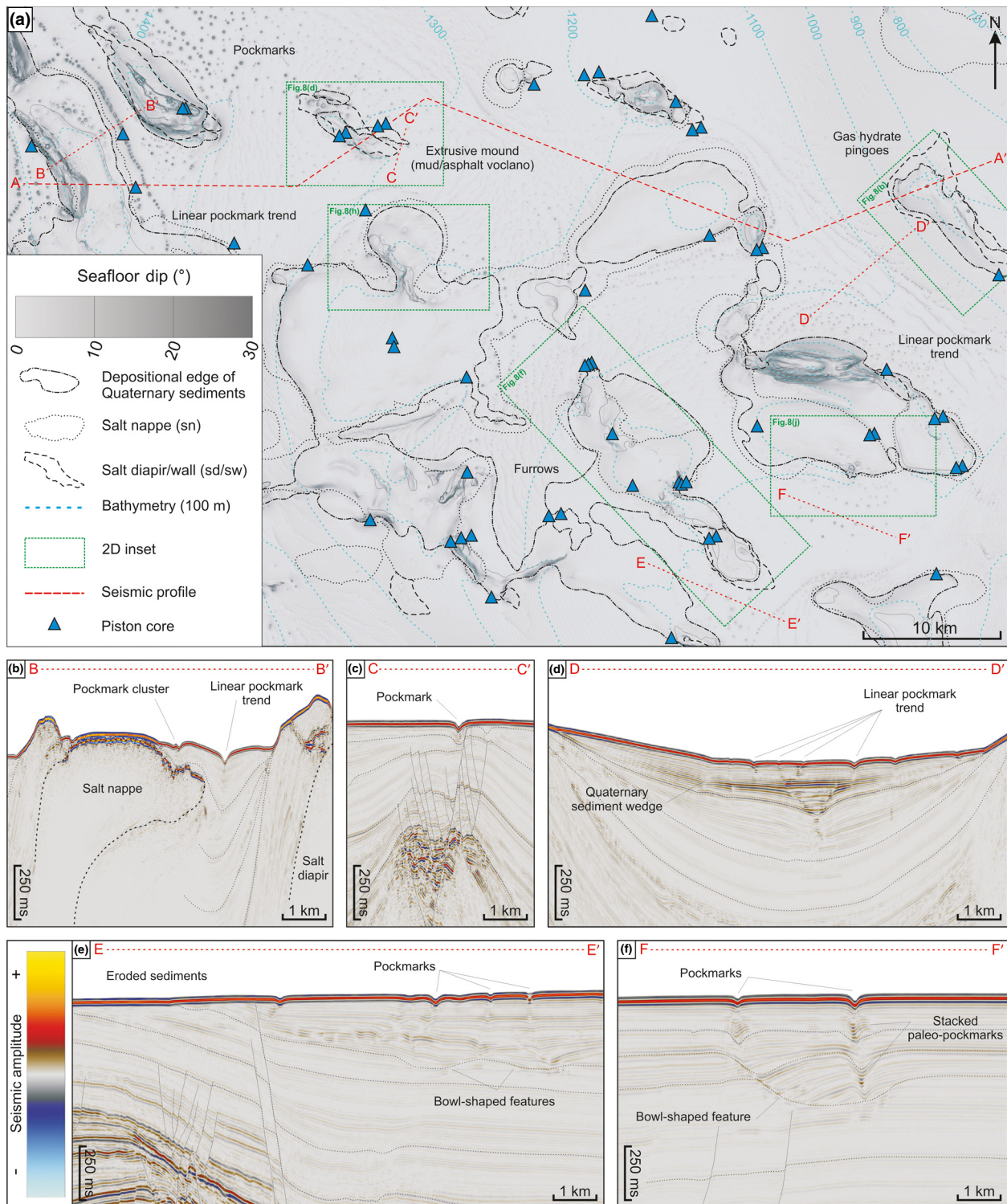
Fig. 7. (a) Seafloor dip map illustrating the presence of numerous bathymetric highs mainly defined by the depositional edge of Quaternary sediments and representing the surface expression of underlying salt diapirs and salt nappes, as well as seep–related seafloor features including pockmarks, linear pockmark trends, extrusive mounds and gas hydrate pingoes. (b–f) Two-dimensional seismic profiles (B–B', C–C', D–D', E–E', and F–F') illustrating relationship between pockmark occurrence with respect to salt structures, faults, recent sediment depocentres and bowl shape features. *Note*: see mounded features on two–dimensional seismic profile on Fig. 10.

is also characterized by a chaotic surface with relatively low amplitudes similar to the surrounding seafloor associated with recently deposited sediment and contrasting with moderate to high amplitudes associated with

exposed older sedimentary rocks cropping out at the seafloor (Figs 6 and 8d, e). Smaller seafloor features characterized by similar chaotic, low amplitude seafloor reflections are also observed on nearby topographic highs
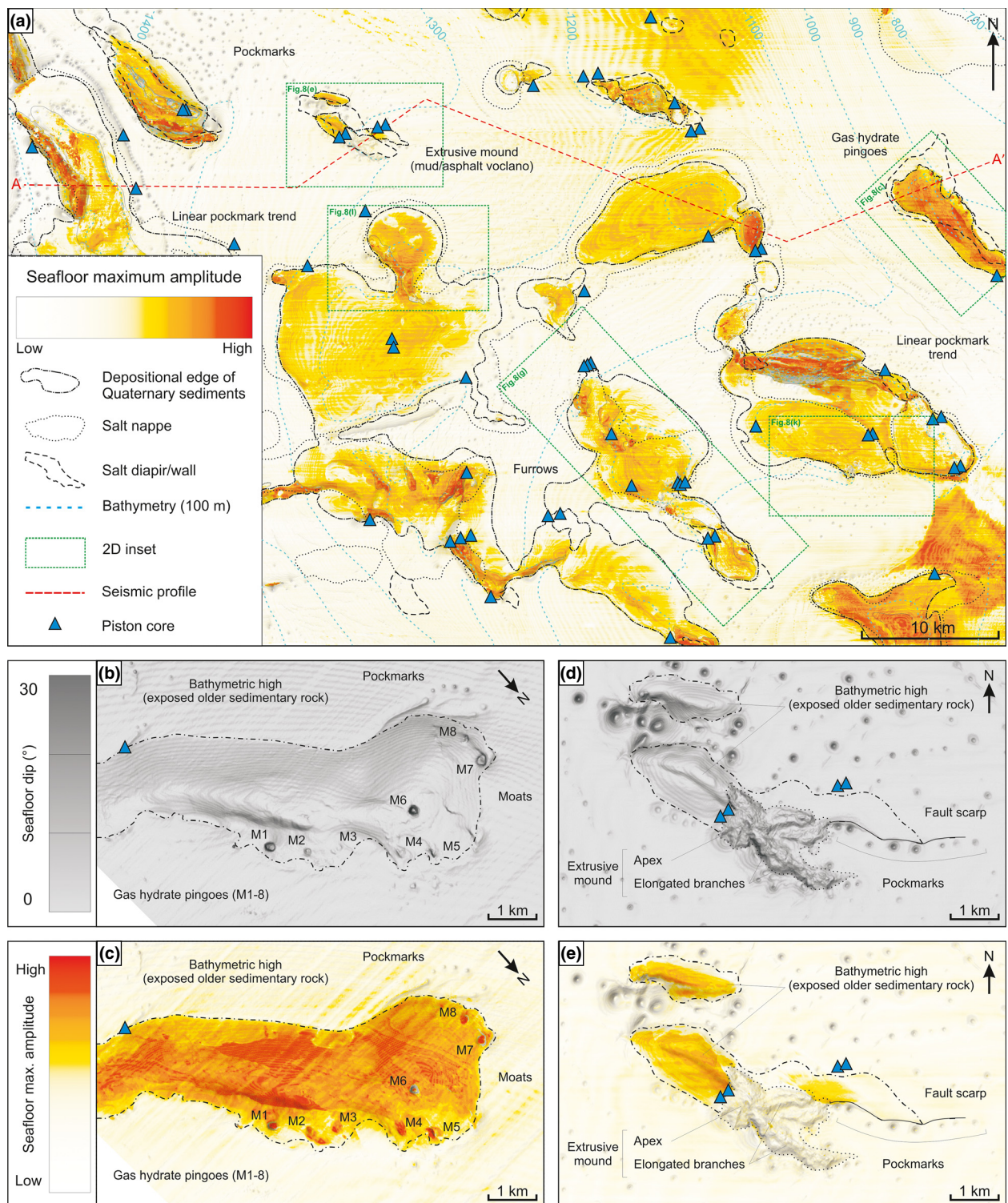
Fig. 8. (a) Seafloor amplitude map illustrating the presence of bathymetric highs associated with high amplitude due to exposed older sedimentary rock and amplitude anomalies associated with seep-related fluid flow features on the seafloor. (b–k) 2D insets illustrating the geophysical signatures of fluid flow phenomena including gas hydrate pingoes and extrusive mounds interpreted as mud or asphalt mound/volcano.

(Fig. 8f–k). Both distinct morphology and geophysical signatures strongly suggest the presence of extruded sediment and fluid expulsion possibly associated with the presence of highly viscous mud or asphalt volcanoes (Kopf, 2002; Evans *et al.*, 2007; Jones *et al.*, 2014).

Overburden fluid flow phenomena

Seismic interpretation of the overburden shows the occurrence of numerous palaeo–fluid flow features and seismic amplitude anomalies, such as palaeo–pockmarks, bottom–simulating reflections (BSRs) and pipes.
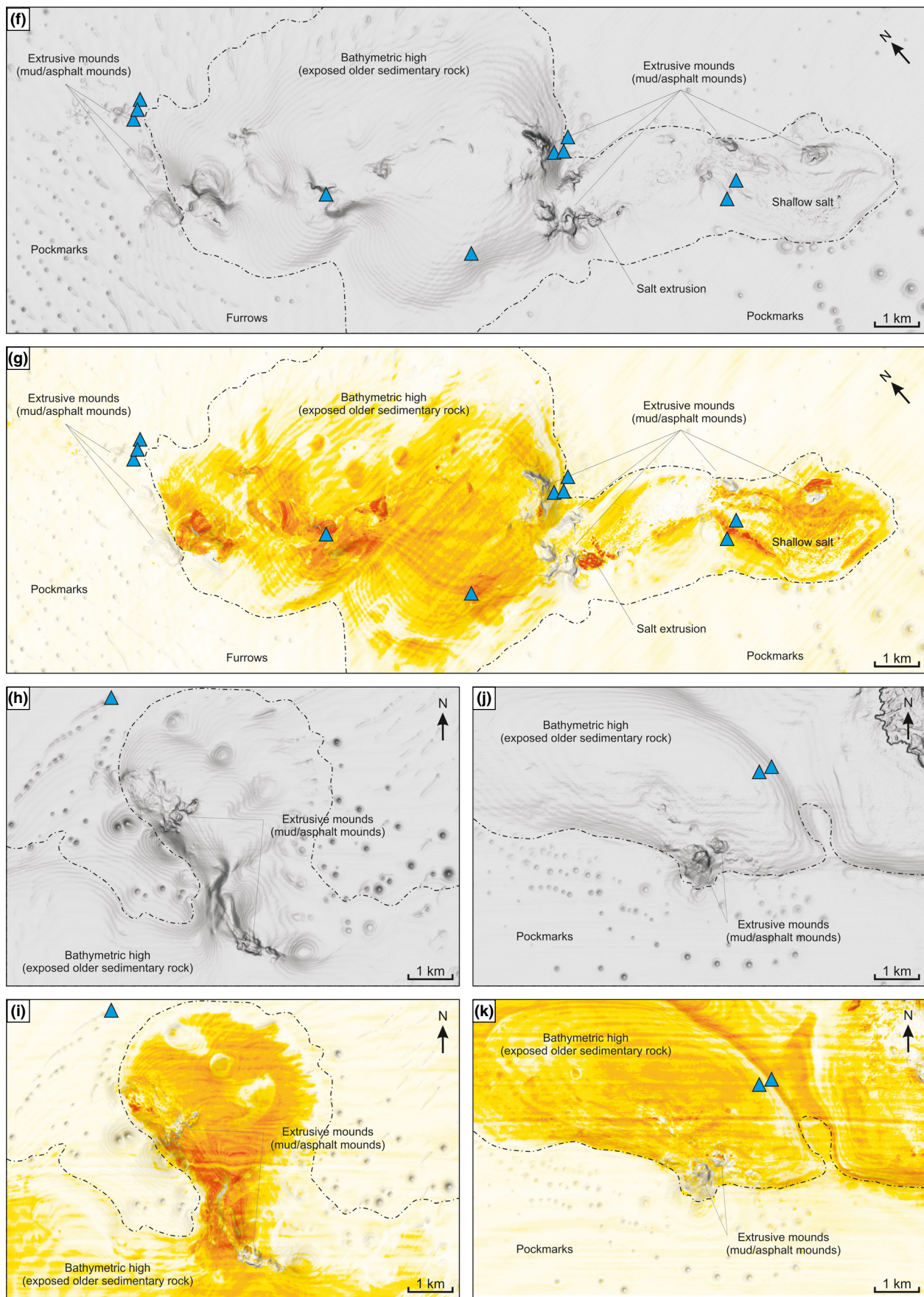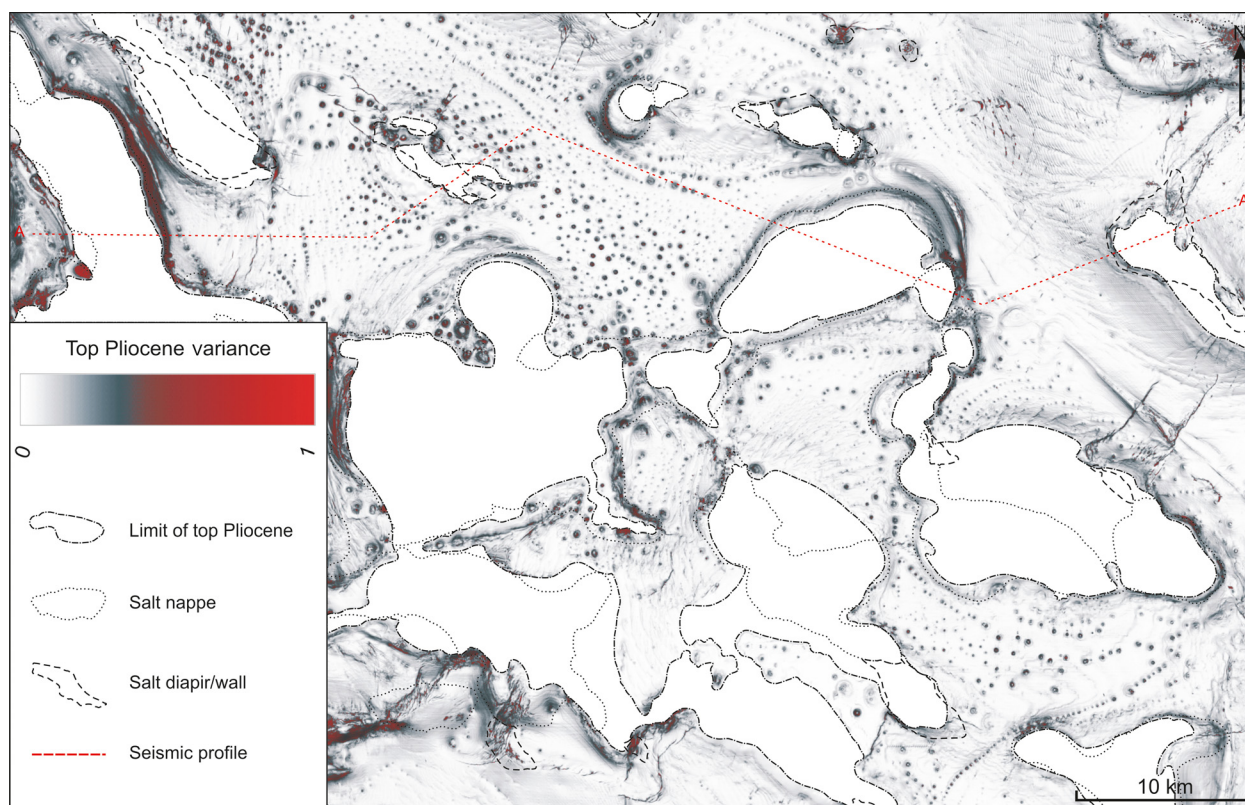
Fig. 8. Continued.

Fig. 9. Variance attribute map along the top Pliocene surface illustrating the presence of numerous palaeo-pockmarks.

Numerous palaeo-pockmarks are clearly imaged at the top of the Pliocene and visualized using a variance attribute along the interpreted surface (Fig. 9). The widespread end-Pliocene pockmarks are opposed to the limited occurrence of individual pockmarks in the deeper section. Palaeo-pockmarks have similar characteristics to present-day seafloor pockmarks, although differences in distribution and intensity might reflect variations between past and present fluid expulsion (Figs 7 and 9).

Seismic anomalies within the shallow subsurface comprise continuous to discontinuous bottom-simulating reflections (BSRs) within minibasins and above salt diapirs (Fig. 10). BSRs within minibasins are defined by a weak negative polarity reflection uniformly mimicking the seafloor topography while crosscutting coherent parallel reflections towards minibasin edges (BSR 1 and 5) between 200 and 280 mbsf. The presence of weak BSRs is enhanced by directly underlying high amplitude reflections confined to particular stratigraphic intervals in minibasins (BSR1 and 5) and bowl-shaped features (BSR 14) most likely representing free gas accumulation in higher permeability layers. Although BSRs usually follow the seafloor topography, they occasionally shoal-up to depths very close to the seafloor when overlying salt diapirs, from depths of 200–280 to 40–100 mbsf (BSR 5, 6, 7, 13, 15, and 16). Above salt diapir, shallow BSRs between 40 and 100 mbsf are characterized by strong, discontinuous, reverse polarity reflections constrained to particular stratigraphic intervals (BSR 13 and 16) as well as along

fault zones, and in some cases directly associated with seafloor fluid flow features (BSR 15 and 16). Geometric relations, reflection coefficients and reflection polarity all support the presence of gas hydrate-related BSRs in the study area.

Additional seismic anomalies consist of stacked high amplitude reflections with pipe-like structures with circular to oval plan view expression varying from 50 to 220 m in diameter and up to 300 ms TWT in vertical extent (Fig. 11). Measured vertical extents are only referring to the high amplitude reflection part, however, vertical size could reach up to 500 ms TWT considering downward blanking. Pipes are generally found above structural highs, and usually associated with faults, unconformities and stratigraphic intervals pinching-out onto structural highs. Pipes are also associated with pockmarks or palaeo-pockmarks (Fig. 11).

Seabed geochemistry

Seabed geochemical analyses consist of 55 piston cores provided by TDI–Brooks International (Table 1). Geochemical interpretation is based on core description, maximum TSF intensity, total alkane gases, sum n-alkanes and UCM concentration in comparison to regional background levels defined from a regional survey including 260 piston cores in the Kwanza Basin.

Piston cores consist predominantly of soft, cohesive, dark greenish clay, with a few composed of hard, stiff
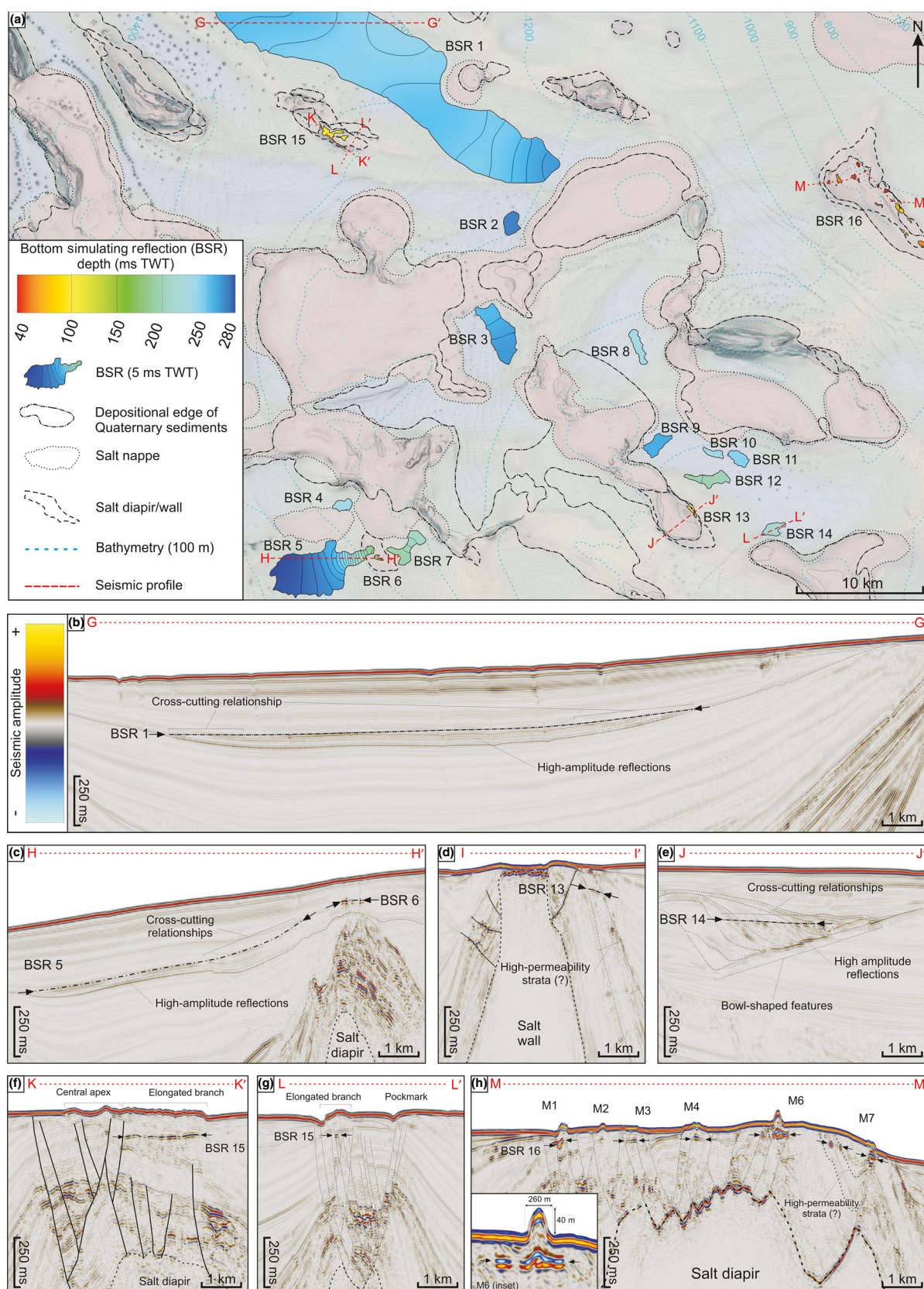
Fig. 10. (a) Bottom simulating reflection (BSR) map illustrating BSR distribution with regard to basin structure and seep-related sea-floor features including pockmarks, extrusive mounds and gas hydrate pingoes. (b–h) Two-dimensional seismic profiles (G–G', H–H', I–I', J–J', K–K', L–L', and M–M') showing BSR occurrences within minibasins (BSR 1), over salt diapir (BSRs 6, 15, and 16), as well as distinct relationship with high-permeability strata (BSR 13 and 16), faults (BSRs 15 and 16) and seep-related seefloor features (BSRs 15 and 16).

Fig. 11. (a) Pipe distribution map compared to top salt structure map and variance attribute map at the top Miocene. (b–g) Two–dimensional seismic profiles illustrating pipe distribu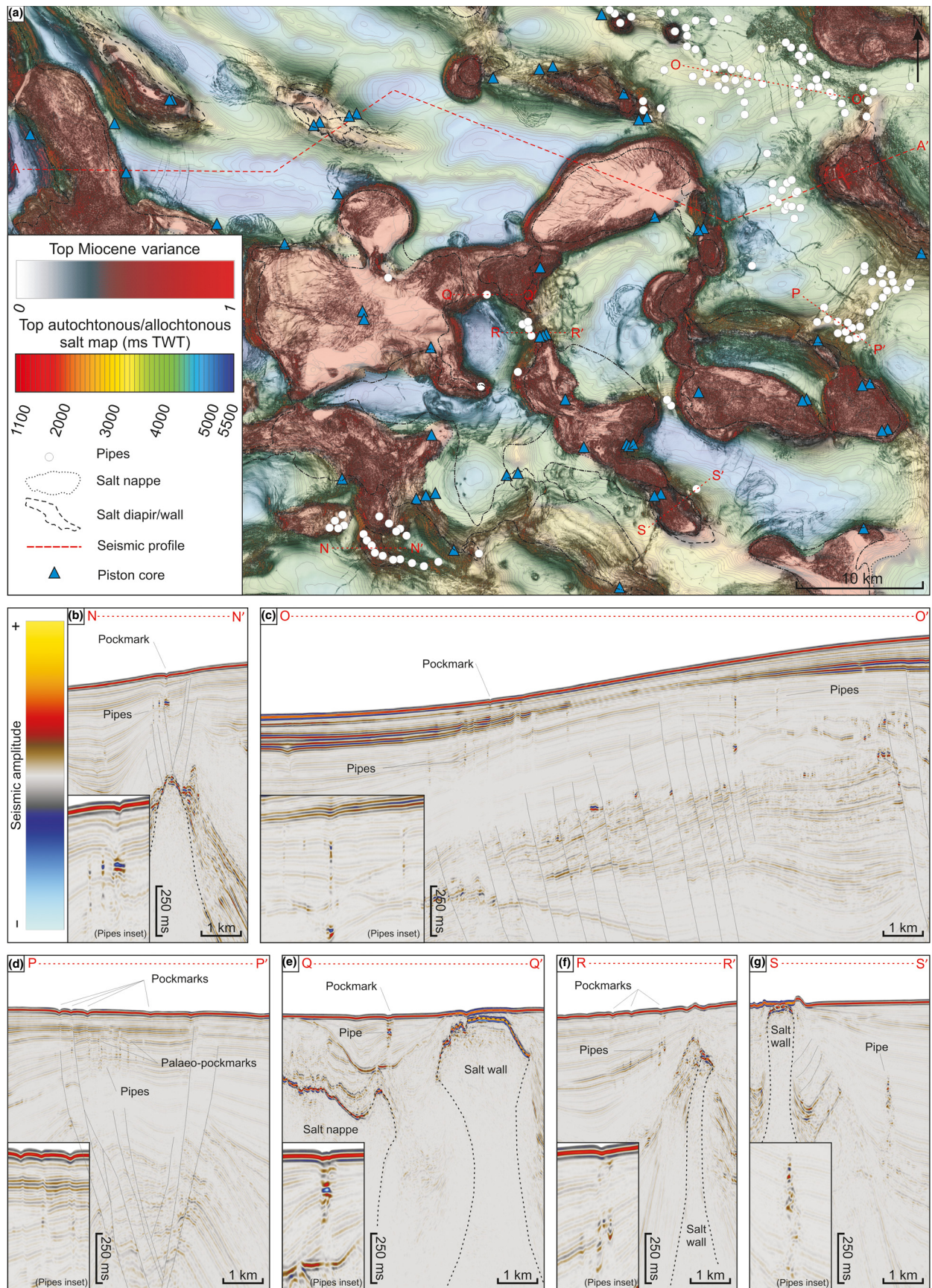tion with regard to salt diapirs (N–N'), faults (O–O' and P–P'), unconformity (Q–Q') and stratigraphic pinch–out onto structural highs (R–R' and S–S').

Table 1. Surface geochemistry data.

CORE No.	SECT	TSF MAX INT	Total Alkane gases (C₁–C₅) (ppmV)	Sum n-Alkanes (C₁₅₊) (ng/g)	UCM (C₁₅₊) (μg/g)
ADW055	09	43 650	25	1105	14
ADW055	13	52 890	20	1255	18
ADW055	17	37 770	39	1142	20
ADW105A	02	72 000	6	2273	56
ADW105A	03	648 600	6	3775	191
ADW105A	05	546 500	12	6032	495
ADW105B	02	152 160	9	8667	568
ADW105B	03	796 200	2	5542	303
ADW105B	05	466 900	2	4048	171
ADW106	13	5594	29	1838	22
ADW106	7	3495	76	2723	32
ADW106	21	3318	26	2139	13
ADW107	10	4152	17	2008	13
ADW107	4	5585	34	2581	18
ADW107	8	5100	47	2442	20
ADW108	12	4604	11	2771	24
ADW108	16	4517	17	1299	15
ADW108	20	3861	28	2220	19
ADW219	15	2850	26	849	15
ADW219	19	3751	51	594	11
ADW219	23	4597	90	931	19
ADW220	10	2968	3	744	12
ADW220	14	2805	6	653	10
ADW220	18	3258	4	2653	24
ADW221	10	3110	8	2277	31
ADW221	14	2961	16	1522	31
ADW221	18	3273	15	1630	40
ADW222	01	2175	2	638	17
ADW222	02	2760	5	651	11
ADW223	01	4889	2	1084	11
ADW223	02	5272	2	860	10
ADW223	03	4179	6	867	9
ADW224	01	1937	3	467	6
ADW225	01	548	4	642	3
ADW225	02	2175	7	914	9
ADW225	03	947	1	2216	16
ADW226	06	2305	2	669	2
ADW226	09	2055	4	1181	8
ADW226	13	2598	2	1138	8
ADW227	12	3028	8	1077	7
ADW227	16	4086	4	1829	29
ADW227	20	3017	15	1952	23
ADW228	08	1487	4	1644	21
ADW228	12	1777	4	1095	15
ADW228	16	2261	2	1223	10
ADW229	13	1956	4	1489	27
ADW229	17	1664	5	1198	27
ADW229	21	3382	8	2270	34
ADW230	15	1874	5	1860	40
ADW230	19	2271	7	2148	37
ADW230	23	2105	8	1713	39
ADW231	10	3183	4	1567	36
ADW231	14	2227	3	1670	44

(continued)

Table 1 (continued)

CORE No.	SECT	TSF MAX INT	Total Alkane gases (C₁–C₅) (ppmV)	Sum n-Alkanes (C₁₅₊) (ng/g)	UCM (C₁₅₊) (μg/g)
ADW231	18	2777	3	1725	33
ADW232	12	4356	4	1277	27
ADW232	16	3359	5	1008	17
ADW232	20	2745	6	1670	48
ADW233	10	1870	13	1176	66
ADW233	14	2769	19	1389	41
ADW233	18	3431	27	2115	47
ADW234	16	2176	13	2192	41
ADW234	20	2074	5	1857	48
ADW234	24	2476	12	2067	45
ADW235A	01	1571	2	1126	33
ADW235A	02	1442	2	923	30
ADW235A	04	2108	3	1075	20
ADW236	06	1864	10	918	12
ADW236	09	1747	10	1344	10
ADW236	13	1477	20	888	9
AS1061	10	1907	3	1755	25
AS1061	14	1166	4	1246	1 5
AS1061	18	2368	7	1281	10
AS1062	10	1695	2	1257	6
AS1062	14	2103	3	1577	15
AS1062	18	6014	5	3661	18
AS1071	11	4261	3	2352	12
AS1071	15	5388	4	2730	16
AS1071	19	2790	4	1653	10
AS1072	13	44580	4	2425	34
AS1072	17	54920	5	2863	52
AS1072	21	3666	5	3947	25
AS1081	10	4134	40	504	11
AS1081	14	11700	122	475	4
AS1081	7	52850	3	435	29
AS1082	14	5648	2	2674	14
AS1082	18	4584	4	824	26
AS1082	22	5646	4	1143	10
AS-1111	11	3220	7	2086	1 3
AS-1111	15	4523	4	1477	11
AS-1111	19	17745	5	1882	18
AS-1112	6	53950	6		59
AS-1112	9	393500	5		94
AS-1112	12	874500	9		229
AS-1113	6	185300	6		63
AS-111 3	8	428000	6		77
AS-111 3	11	450100	9		123
AS-1121	10	3150	4	862	7
AS-1121	14	5408	5	1990	15
AS-1121	18	5266	12	2631	16
AS-1122	12	2368	4	1302	10
AS-1122	16	3872	4	1687	17
AS-1122	20	4269	5	1137	11
AS-1131	7	4353	4	851	9
AS-1131	11	3663	9	969	11
AS-1131	15	4795	10	2197	15
AS-1132	10	32590	5	1091	11
AS-1132	14	3559	7	1083	11

(continued)

Table 1 (continued)

CORE No.	SECT	TSF MAX INT	Total Alkane gases (C$_1$–C$_5$) (ppmV)	Sum n-Alkanes (C$_{15+}$) (ng/g)	UCM (C$_{15+}$) (μg/g)
AS-1132	18	3520	8	2066	17
AS-1141	6	1662000	8		303
AS-1141	9	1097500	8		132
AS-1141	12	790000	5		95
AS-1142	11	902500	6		141
AS-1142	15	450300	6		122
AS-1142	19	496400	3		115
AS-1143	6	865500	6		176
AS-1143	9	517600	5		141
AS-1143	13	99620	5	4169	55
AS-1151	12	47820	5	1446	40
AS-1151	16	38440	5	2184	19
AS-1151	20	15885	5	1352	14
AS-1152	12	35170	5	2014	43
AS-1152	16	36580	6	1139	13
AS-1152	20	20845	4	2478	21
AS-1161	7	3028	4	1067	8
AS-1161	10	2700	3	1397	1 3
AS-1161	14	2639	5	1084	16
AS-1162	1	4106	3	709	8
AS-1162	2	4042	4	374	23
AS-1162	4	1978	3	306	9
AS-1163	1	1626	5	253	5
AS-1163	2	881	0	226	8
AS-1211	6	3145	2	1228	11
AS-1211	9	3692	4	1688	1 3
AS-1211	12	3177	4	1987	17
AS-1212	5	3110	2	816	4
AS-1212	7	2840	2	691	8
AS-1212	10	3325	5	927	6
AS-1221	12	1916	5	957	10
AS-1221	16	1971	8	1880	23
AS-1221	20	3097	14	2462	12
AS-1222	11	2099	3	754	10
AS-1222	15	1819	10	819	9
AS-1222	19	3152	10	2851	14
AS-1231	9	17910	5	952	11
AS-1231	13	20640	4	1660	14
AS-1231	17	42130	10	2179	18
AS-1232	9	5291	5	1331	11
AS-1232	13	5746	7	1337	8
AS-1232	17	3906	9	1773	14
AS-1241	5	3459	4	966	11
AS-1241	7	2874	3	1268	26
AS-1241	10	2692	2	1005	9
AS-1242	6	2138	6	863	11
AS-1242	9	1882	5	1185	7
AS-1242	13	2887	6	1844	11
AS-1251	6	51340	3	744	1 5
AS-1251	9	3676	4	832	6
AS-1251	12	2608	3	763	4
AS-1252	10	60880	3	1016	22
AS-1252	14	40740	5	1333	17
AS-1252	18	47490	4	3214	31

clay. Lithological description also includes information on direct evidence supporting the presence of migrated thermogenic hydrocarbon such as black streaks (AS-1081, AS-1082, AS-1141, AS-1151, AS-1162) and asphalt inclusions (AS-1112, AS-1113, AS-1141, AS-1143).

The TSF data for the study area varies between 548 and 1 662 000 units (Table 1, Fig. 12); with 25% of the 161 analysed sediment extracts having maximum TSF intensities greater than background level for the region (less than 10 000 units). Sixteen piston cores with maximum TSF intensities greater than 10 000 units (ADW055, ADW105A, ADW105B, AS1072, AS1081, AS-1111, AS1112, AS1113, AS1141, AS1142, AS1143, AS1151, AS1152, AS1231, AS1251, AS1252) show evidence of migrated thermogenic hydrocarbons in near surface sediment (Fig. 12).

Headspace gas analysis of sediment samples shows light hydrocarbon concentration between 1 and 90 ppmV reflecting background levels characteristic of marine sediments, in addition to low concentration of C$_{2+}$ alkane (Table 1 and Fig. 13). Light hydrocarbon concentration greater than 100 ppmV and high concentration of C$_{2+}$ suggest the presence of migrated thermogenic hydrocarbons since ethane, propane, butane and pentane are not microbially produced at high level in marine sediments (Abrams, 2005).

C$_{15+}$ analysis provides n-alkane and UCM concentrations, as well as gas chromatograms. The concentration of n-alkanes in sediment extract in the study area varies between 467 and 8667 ng/g (Table 1, Fig. 14). UCM concentration are ranging from 2 to 568 ng/g (Table 1, Fig. 15), with 9% of the 161 analysed sediment extracts having UCM concentration above the regional background (100 ng/g).

Gas chromatograms are classified into three types determined from the levels of the UCM baseline, relative enrichment in long-chain n-alkanes and even/odd carbon predominance (Fig. 16). All gas chromatograms show peaks labelled IS and SU representing internal and surrogate standards added as part of the analytical method, as well as an accentuated base line signature usually reflecting low sample concentration at higher temperature (Fig. 16b–d). Type 1 gas chromatograms are characterized by a complete sequence of n-alkanes, elevated UCM baseline and C$_{23}$–C$_{35}$ *n*-alkanes with some predominance of even over odd carbon numbers, and are usually associated with a UCM 'hump' depending on the degree of biodegradation (Fig. 16b). Type 2 gas chromatograms are also characterized by a complete sequence of *n*-alkanes with relatively low peaks in low chain hydrocarbons, as well as a lower UCM base line (Fig. 16c). Type 3 gas chromatograms are defined by a low UCM baseline and an enrichment in long-chain n-alkanes (<n-C$_{23}$) with odd carbon preference (n-C$_{27}$, n-C$_{29}$, n-C$_{31}$) (Fig. 16d). Type 1 shows significant evidence for the presence of migrated thermogenic hydrocarbons, as opposed to type 3 directly associated with recent, terrigenous organic matter. Type 2 is most likely associated with terrigenous organic mat-
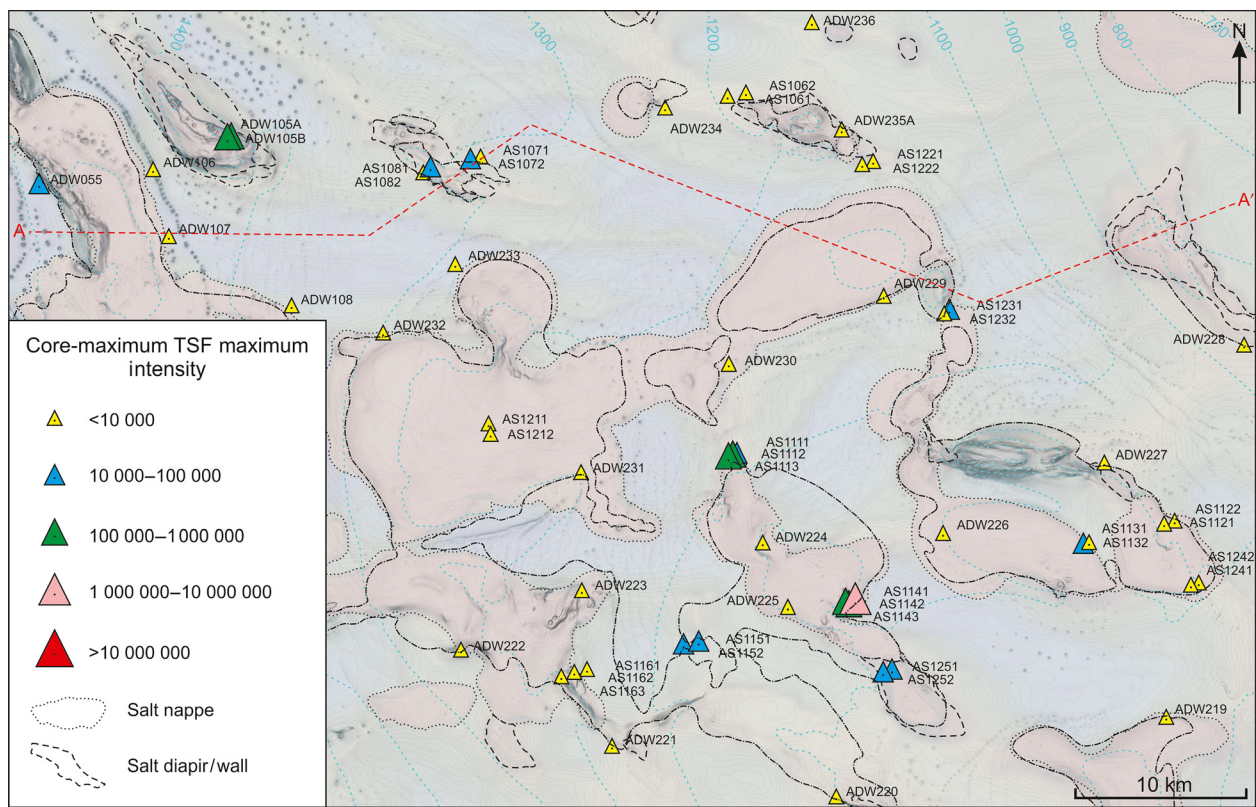
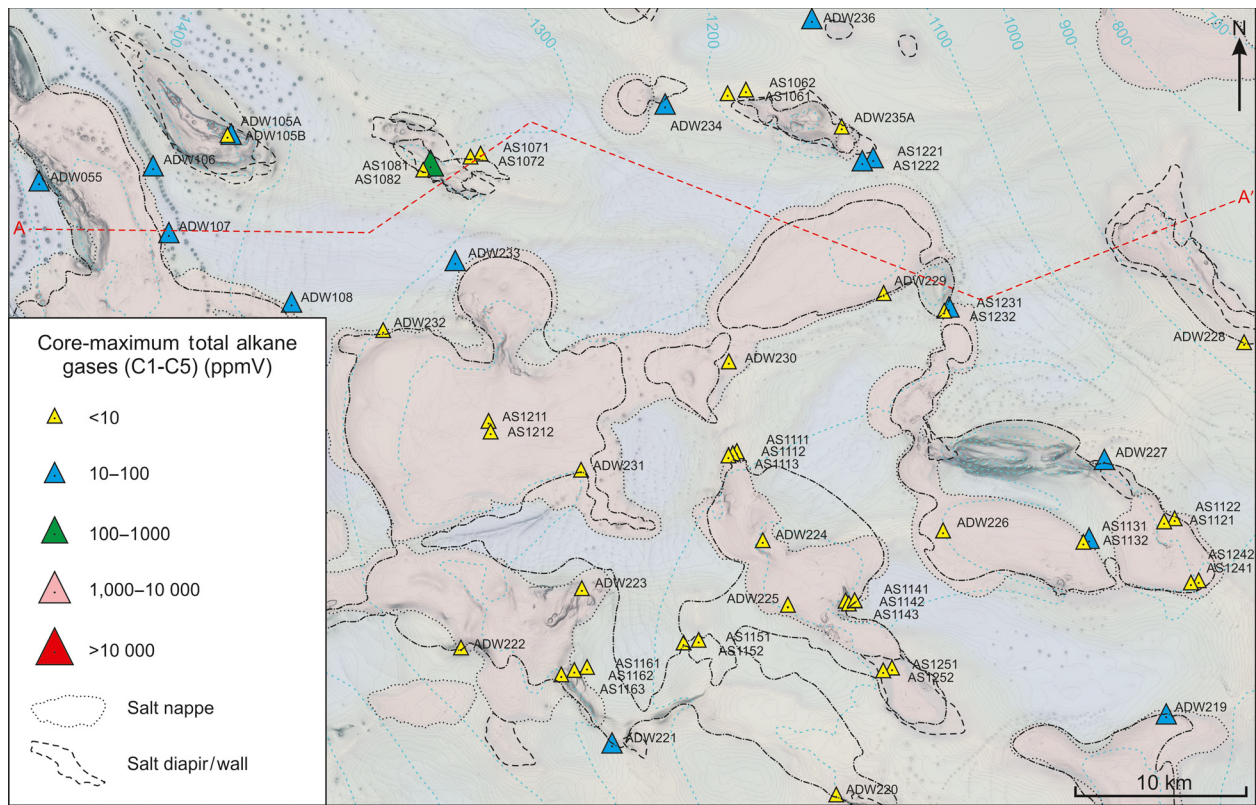**Fig. 12.** Core–maximum total scanning fluorescence (TSF) map.

Fig. 13. Core–maximum total alkane gases (C_1–C_5) (ppmV) map.
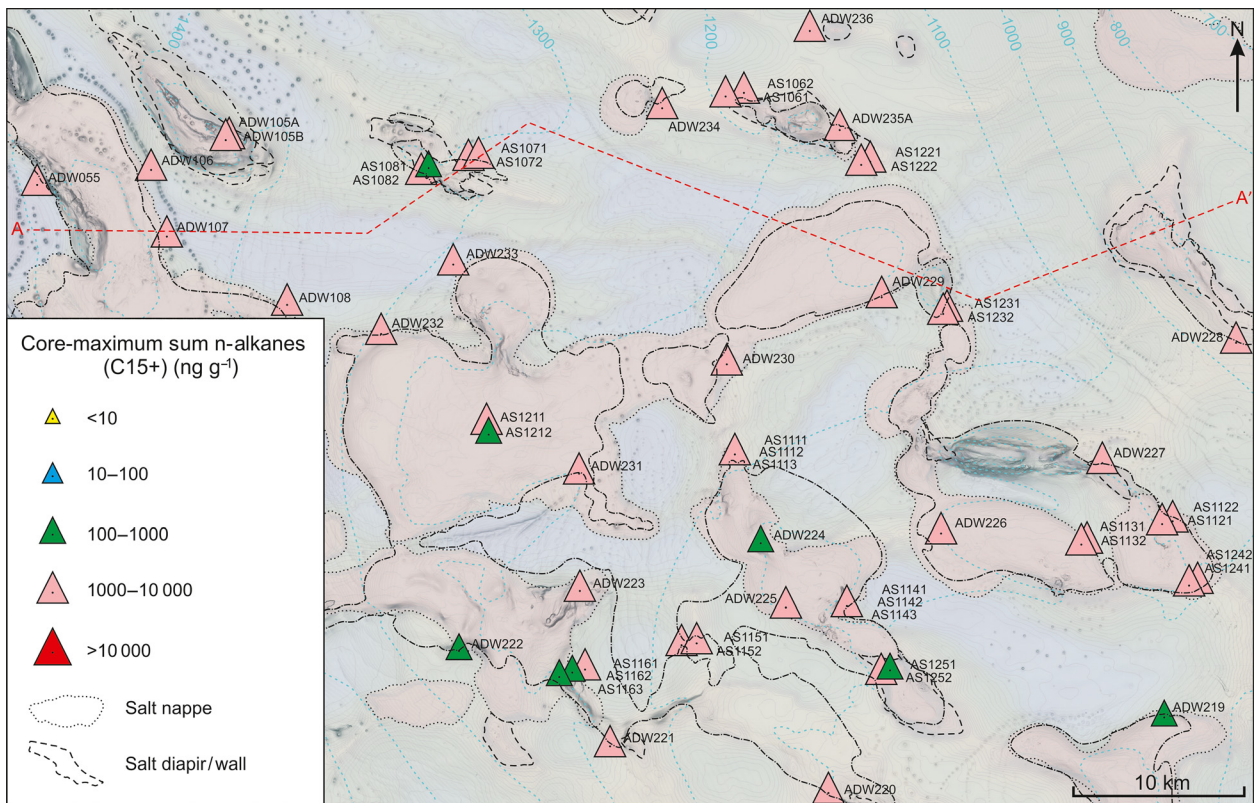
Fig. 14. Core-maximum Sum *n*-Alkanes (C$_{15+}$) (ng/g) map.
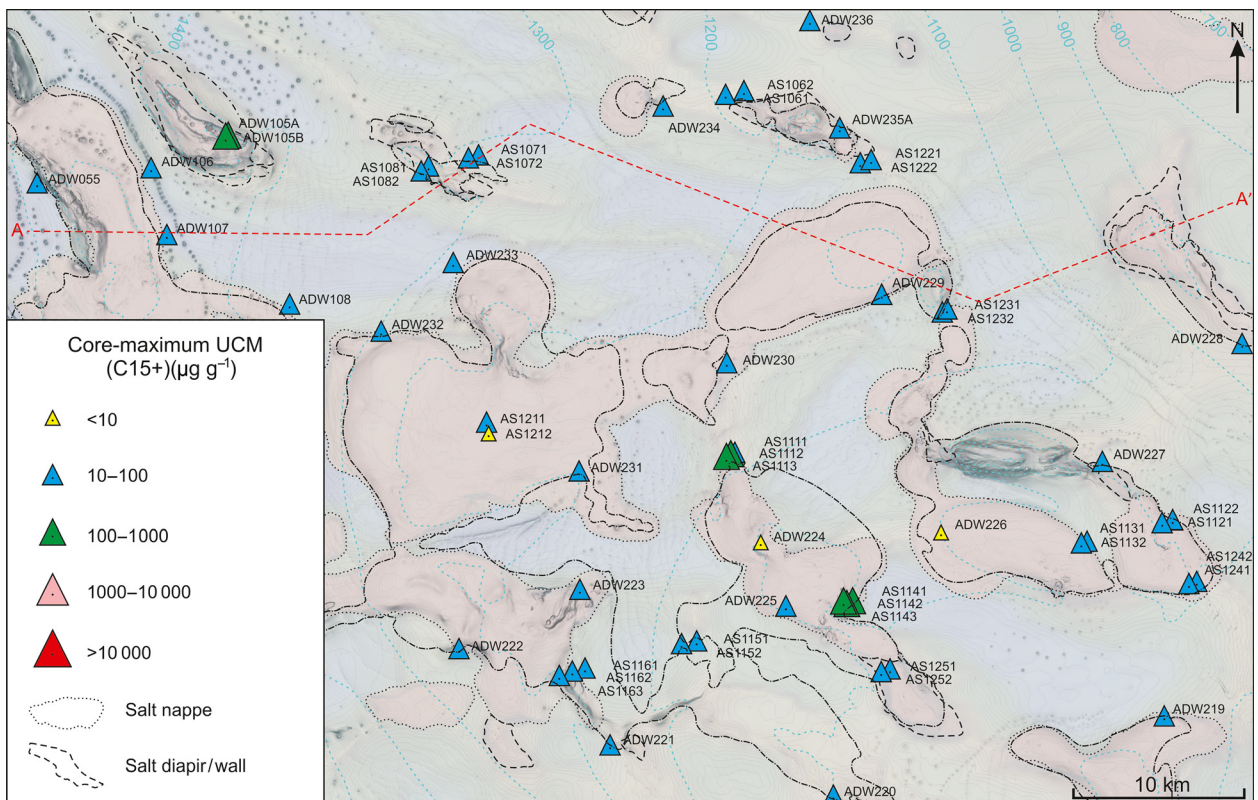

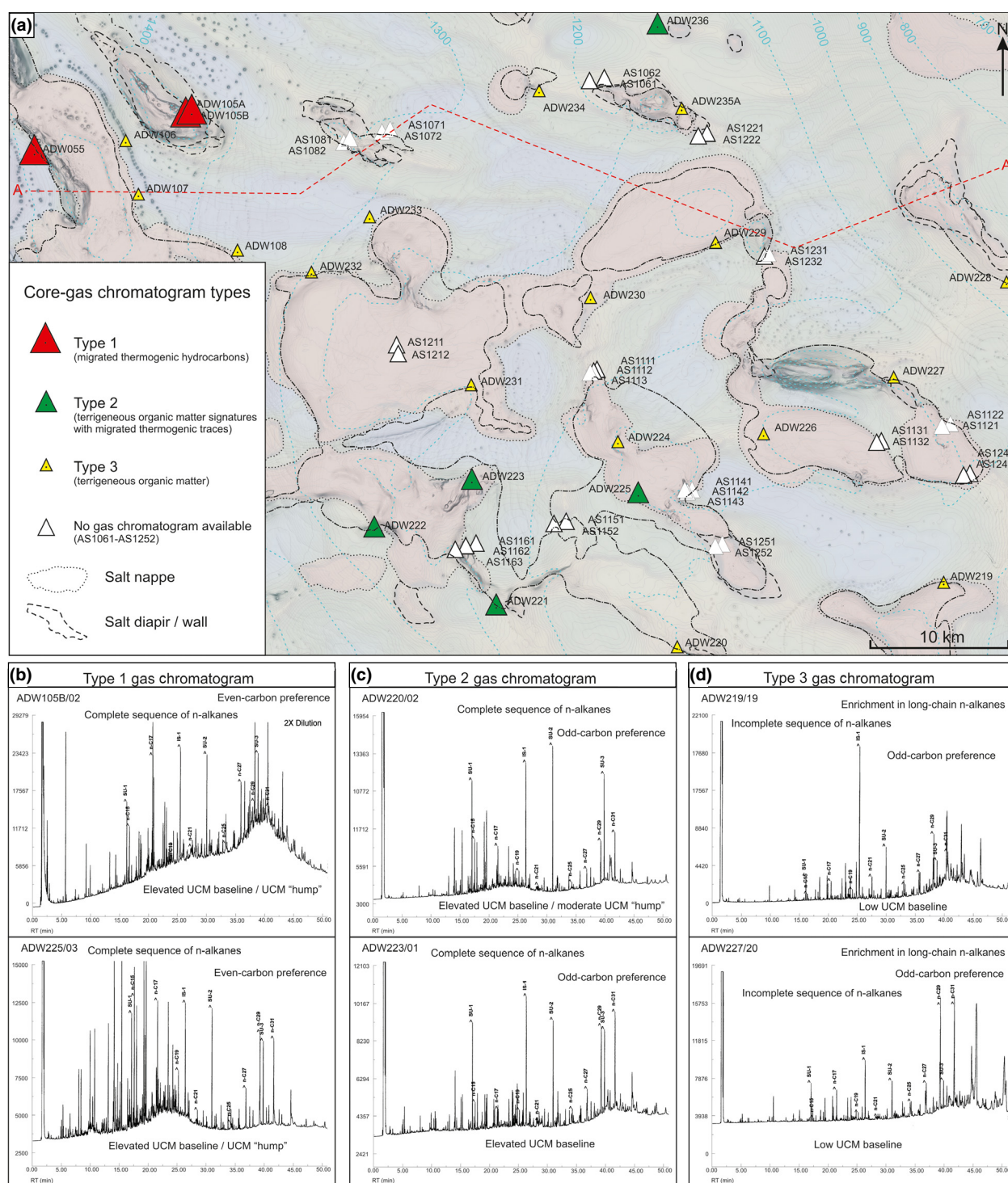**Fig. 15.** Core-maximum unresolved complex mixture (UCM) (C$_{15+}$) (ug/g) map.

Fig. 16. (a) Gas chromatogram map classified by types based on n-alkanes sequence, UCM base line, even/odd carbon preference, and enrichment in long chain n-alkanes. (b) Type 1 associated with migrated thermogenic hydrocarbon. (c) Type 2 showing potential evidence for migrated thermogenic hydrocarbons and (d) Type 3 representing recent, terrigeneous organic matter.

ter; however, some evidence suggests the possibility of thermogenic hydrocarbon occurrence.

Overall, sections from nine piston cores (ADW055, ADW105A, ADW105B, AS1081, AS1112, AS1113, AS1141, AS1142, AS1143) show clear evidence for the presence of migrated thermogenic hydrocarbons in near-surface sediments based on high TSF, UCM and GC characters, as well as the presence of black streak and asphalt inclusions. Additionally, 10 piston cores (ADW221, ADW222, ADW223, ADW225, ADW236, AS1072, AS1082, AS1111, AS1132, AS1151, AS1152, AS1231, AS1251 and AS1252) indicate possible evidence for thermogenic hydrocarbons, as opposed to 36 cores directly associated with terrigenous organic matter. The
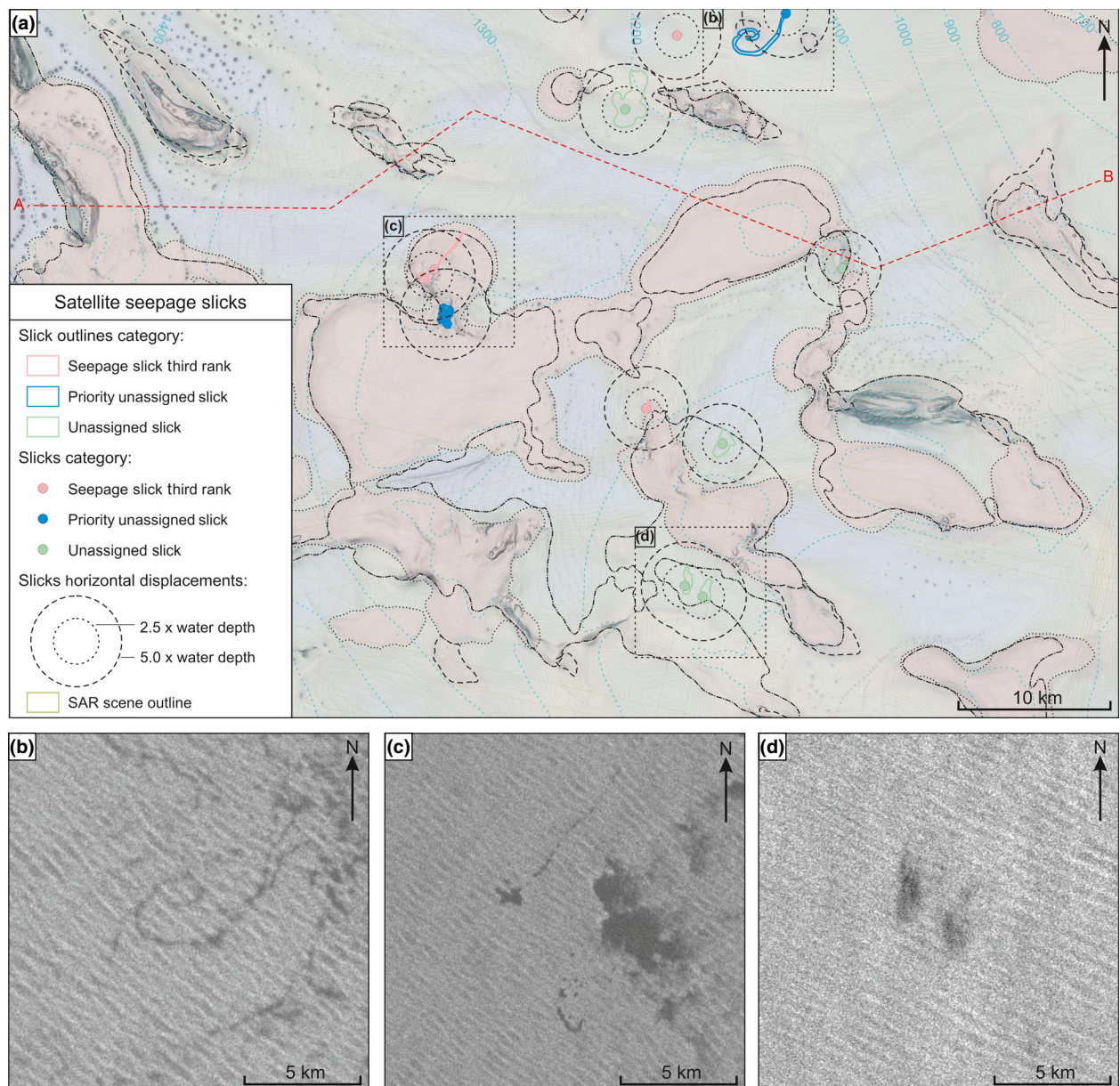
Fig. 17. (a) Satellite seepage slick interpretation map showing clustered slicks including slick outlines, emission points, interpreted categories (third rank, priority unassigned and unassigned slicks), as well as range of lateral displacement based on 2.5 and 5 times the water depth. (b–d) SAR scene insets showing seepage slicks characteristics (elongated drift across swell, corkscrew habit or clusters of variable sizes).

origin of migrated thermogenic hydrocarbons in cores ADW055, ADW105A and ADW105B is difficult to classify because of their mixed signal with immature recent sediments. Further geochemical analyses suggest a post-salt marine origin, but a possible contribution from lacustrine source rocks beneath the salt layer cannot be eliminated.

Satellite-based surface slicks

Analysis of 12 SAR scenes each partially covering the study area show the presence of 16 clustered slicks with interpreted slick outlines and emission points (Fig. 17). Slicks appear as regions of dark smooth textures on satel- lite images and interpreted seepage slicks are usually char- acterized by the presence of distinct emission points with elongated drift across swell (Fig. 17c), corkscrew habit (Fig. 17b), or clusters of variable sizes (Figs 17c, d). Interpreted slicks consist of four third-rank slicks, seven priority-unassigned slicks and five unassigned slicks (Fig. 17a). Third-rank slicks are defined as potential seepage slicks with 40% confidence of them being actual seepage slicks. Priority unassigned slicks and unassigned slicks are interpreted as seepage with 20% and 10% confi- dence. However, low confidence levels do not represent negative results in sparsely surveyed areas. Additional integration with geological and geochemical data and analysis of repeated overlapping scene provide significant
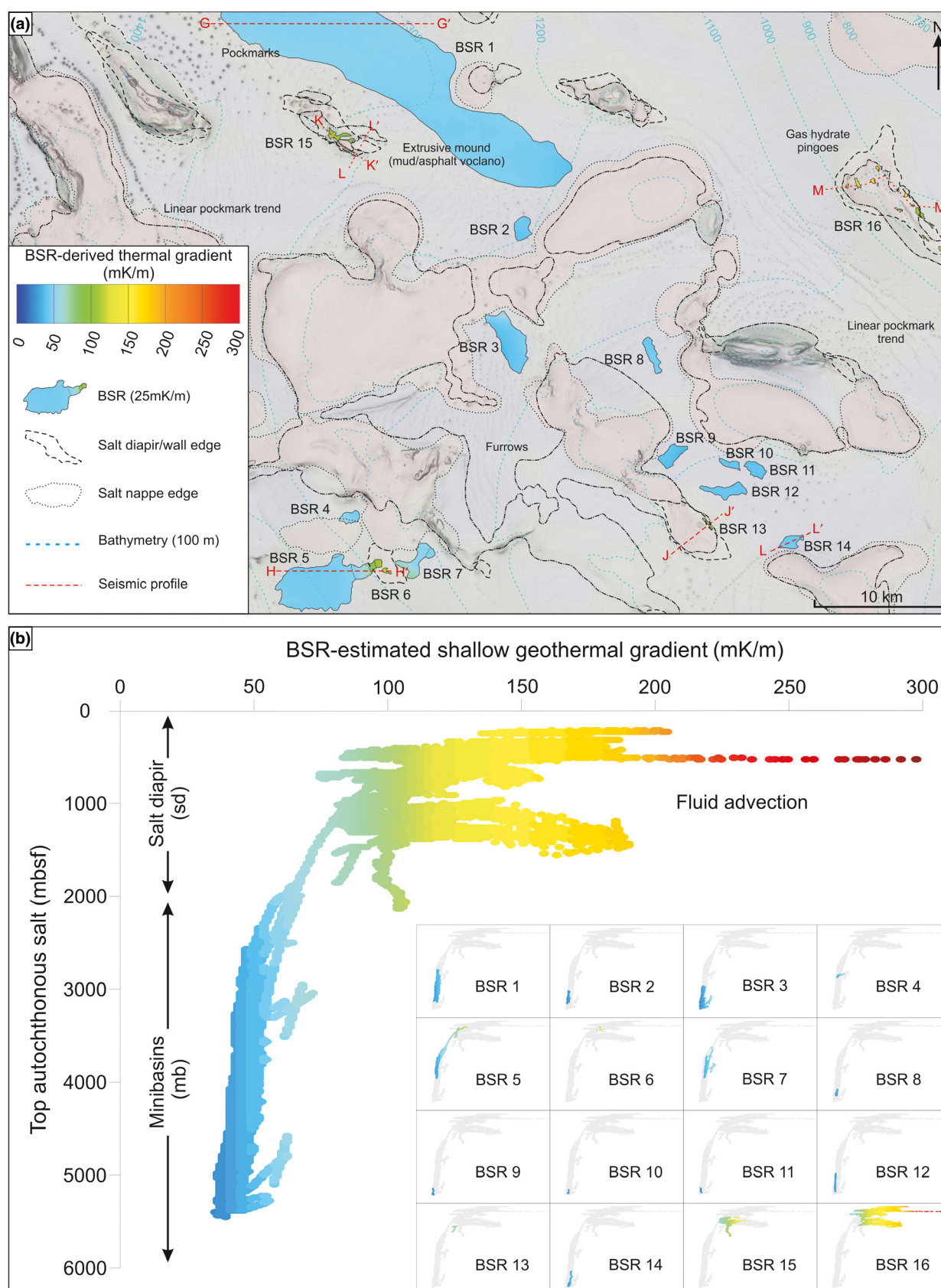
Fig. 18. (a) Bottom simulating reflection–derived shallow thermal gradient map illustrating gradient variation with respect to basin structure and seep-related seafloor features including pockmarks, extrusive mounds (mud/asphalt volcanoes) and gas hydrate pingoes. (b) Comparison of BSR–derived shallow geothermal gradient (mK/m) with salt depth (mbsf) illustrating estimated shallow geothermal gradient with regard to the proximity of highly conductive salt, as well as fluid advection associated with seafloor seeps.

BSR-derived shallow geothermal gradient

Based on the gas hydrate stability conditions, the presence of gas hydrate-related BSRs within the study area provides a means of estimating shallow geothermal gradients and subsequently determining the occurrence and origin of shallow thermal anomalies. BSR-derived shallow geothermal gradients within the study area vary between 36 mK/m and 300 mK/m with relatively low gradients within minibasins and anomalously high gradients above salt diapirs (Fig. 18). BSR-derived shallow geothermal gradients within minibasins are consistent with a published borehole measurement in the nearby Benguela Basin where a geothermal gradient of 46 mK/m (or 46°C/km) was measured at ODP Leg 175–1078 for the uppermost 130 m below seafloor (Fig. 1) (Party, 1998). Shallowing BSRs above salt diapirs have previously been documented in the Lower Congo Basin and attributed to thermal conductivity contrast between rock salt and siliciclastic strata (Lucazeau *et al.*, 2004). The presence of rock salt with high thermal conductivity (~6.5 W/m.K) compared to mudstone (1.5–2.5 W/m.K) and sandstone (1.5–3.0 W/m.K) can result in anomalous surface heat flow up to three times greater than that experienced away from salt structures (Von Herzen *et al.*, 1972; Nagihara *et al.*, 1992). Comparison of BSR-derived shallow geothermal gradients with respect to top salt depth (mbsf) shows strong relationships where shallow geothermal gradients are relatively constant (45–55 mK/m) between 5500 and 2000 mbsf (BSR 1–4, 8–12, 14), increasing gradients associated with shallower salt structure between 4000 and 500 mbsf (BSR 5 and 7), and relatively high gradients (>75 mK/m) over salt diapirs between 2000 and 500 mbsf (Fig. 18).

In the absence of local seabed heat probe measurements and lack of access to exploration borehole temperatures in the study area, a qualitative comparison with shallow geothermal gradients derived from existing conventional thermal models and a recently compiled global heatflow database (Davies, 2013) shows similar results reflecting an overall heat flow of about 40–50 mW/m^2 and a significant effect of highly conductive salt (Fig. 18). Average shallow geothermal gradients within the upper 400 mbsf shows similar results reflecting the effect of highly conductive salt with relatively increasing gradient over shallow salt structures up to 150 mK/m (BSR 5, 6 and 7) (Fig. 18). The minibasin thermal gradient of 35–50 mK/m measured for the GHSZ would correspond to heatflow of 35–65 mW/m^2 for thermal conductivities of 0.8–1.0 W/m.K, as measured for the upper section of ODP Site 1078 (Party, 1998). These values are in agreement with heatflow values measured in the area (Davies, 2013).

The occurrence of anomalously high BSR-derived shallow geothermal gradients (<120 mK/m) over salt diapirs

(BSR 15 and 16) can be directly associated with highly conductive salt structure, as well as the possible effect of fluid advection along deep-rooted plumbing systems as shown by the presence of patchy and local BSR, as well as distinct seep-related seafloor features including pockmarks, mud volcanoes and gas hydrate pingoes (Figs 7 and 8). Fluid advection around salt diapirs is generally associated with deeply buried and relatively warm brines and hydrocarbon fluids (Aharon *et al.*, 1992; MacDonald *et al.*, 2004). In the absence of direct fluid composition measurements, the present estimation of BSR-derived shallow geothermal gradients should be considered as a preliminary approach based on a simple salinity and methane system while considering the effect of fluid composition on the stability of gas hydrates (Holder *et al.*, 1987; Dickens & Quinby–Hunt, 1994). For instance, an increase in salinity would result in a slight shallowing of the gas hydrate stability zone, whereas the presence of higher hydrocarbon proportion would increase the stability of gas hydrates, pushing the basal limit deeper into the subsurface. Changes in gas hydrate stability conditions will subsequently result in relatively warmer or colder temperature estimations at BSR-depth, and hence relatively higher or lower shallow geotherm estimations. Finally, comparison of BSR-derived shallow geothermal gradients to top salt depth (mbsf) shows that BSR-derived shallow geothermal gradients associated with seep-related fluid flow features have a relatively higher thermal gradient compared to those associated with stratigraphic intervals. This may be due to a combination of fluid advective effects and thermal conductivity variations linked with enhanced gas hydrate concentrations (Serié, 2013).

DISCUSSION

Integrated analyses of fluid flow

This study utilizes data of different vintages and variable coverage including 3D seismic, seabed geochemistry and satellite-based surface slick. The iterative workflow used here augments the interpretation of individual data types and provides an integrated analysis that helps overcome the limitations of individual datasets while also highlighting additional data required for a complete characterization of the local fluid flow system in the deep-water Kwanza Basin (Figs 19 and 20). The approaches outlined herein are adaptable and applicable to any frontier basin.

Seismic interpretation calibrated to nearby exploration wells helped to constrain the tectono-stratigraphic framework within the study area, including the presence of source rock, aquifer, sealing units, as well as structural deformation dominated by salt tectonics. High-quality and relatively high definition 3D seismic provided a detailed picture of surface manifestations of fluid expulsion and associated overburden anomalies (pockmarks, gas hydrate pingoes, authigenic carbonates, mud volcanoes, asphalt volcanoes, DHIs, BSRs, pipes/chimneys). In addition, overburden seismic interpretation provided
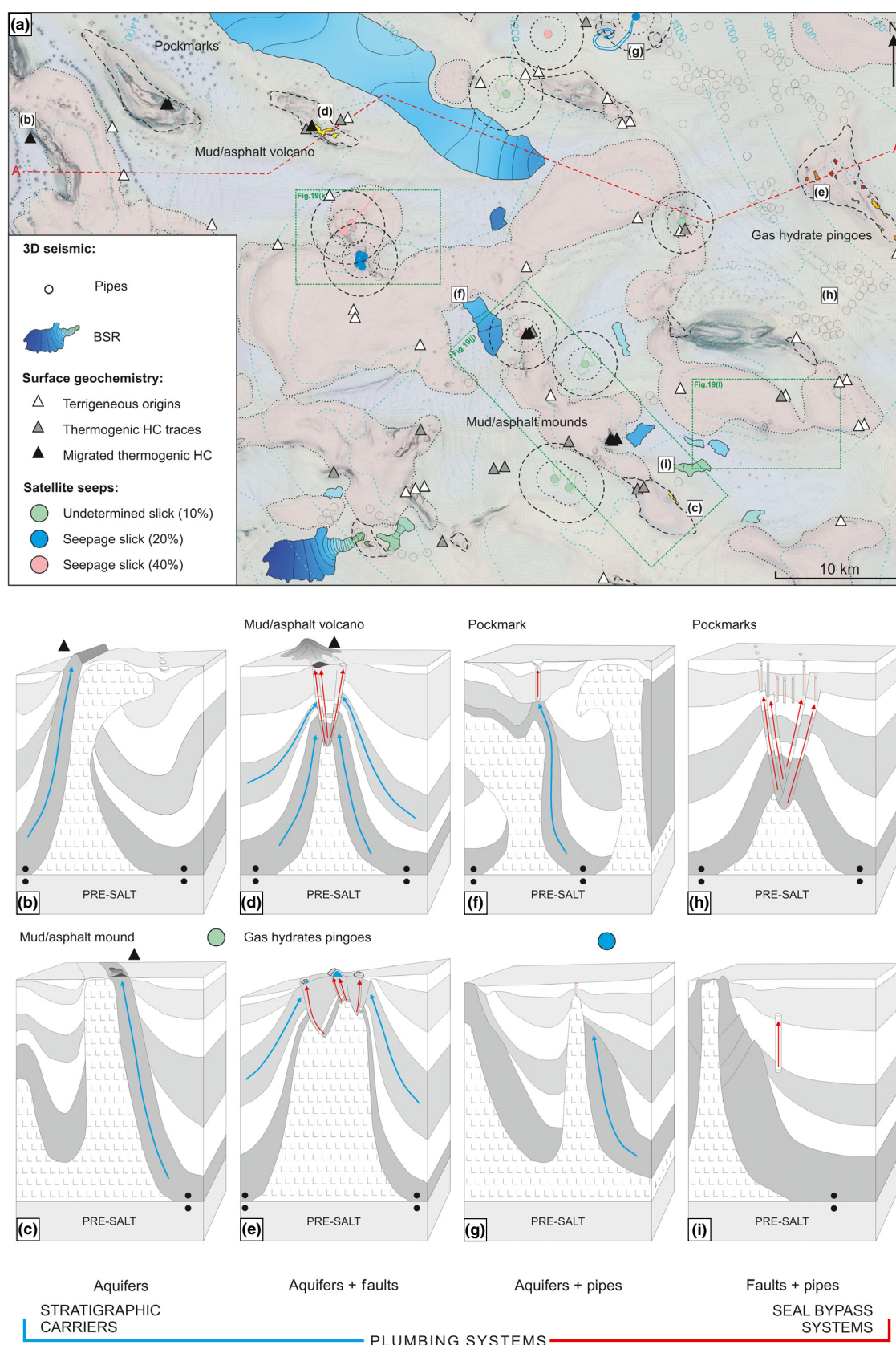
Fig. 19. (a) Integrated map of fluid flow phenomena studies illustrating both consistency and complementarity between seismic, sur-face geochemistry and seepage slick analysis. (b–i) Schematic representations of observed fluid flow phenomena illustrating the pres-ence of deep-rooted plumbing systems characterized by the stratigraphic carriers and seal bypass systems (faults and pipes), as well as salt welds potentially enhancing hydrocarbon migration from pre-salt source rocks into the post-salt interval.(j–l) 2D insets illustrating the complementarity between data sets.
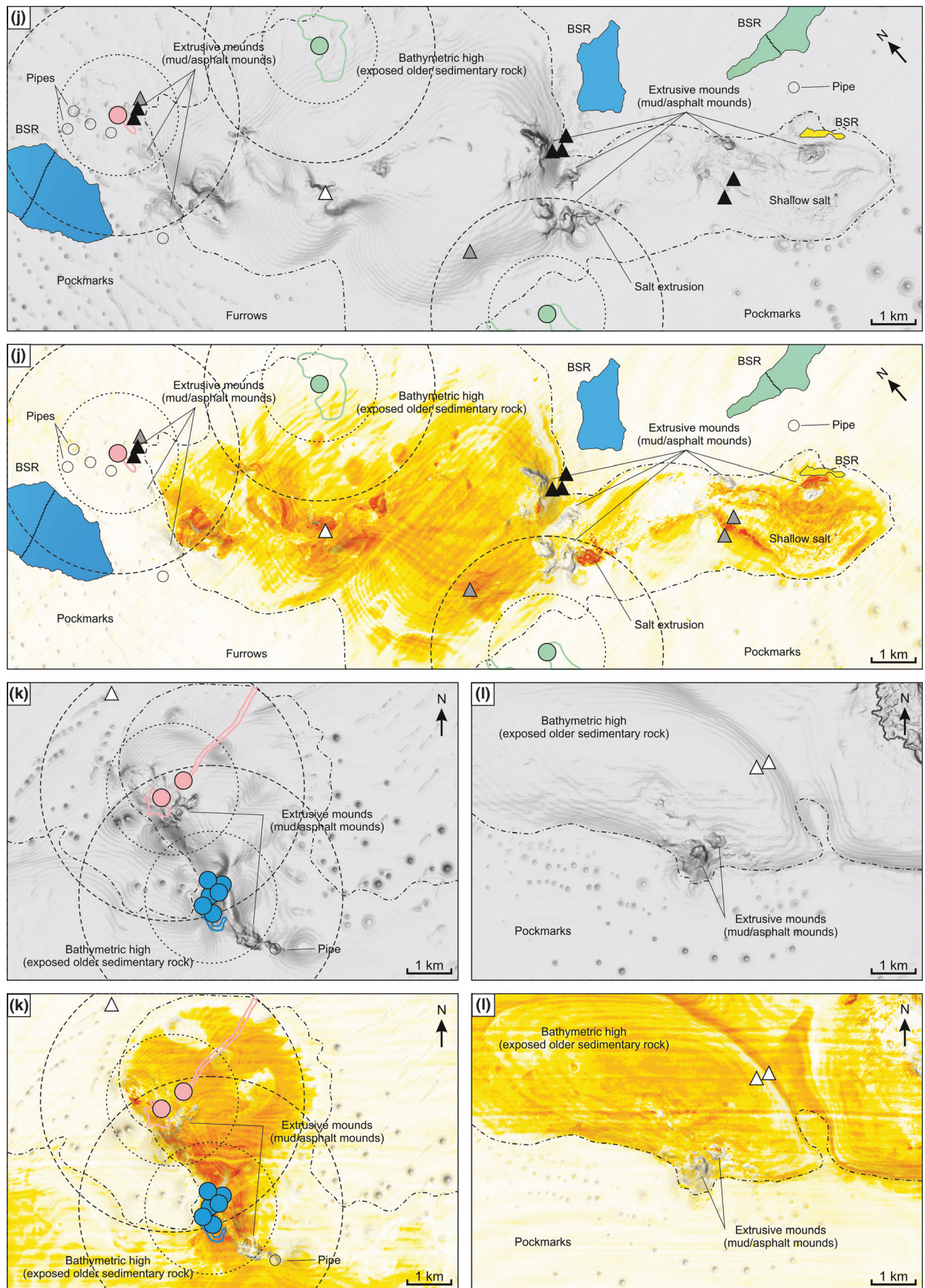
Fig. 19. Continued

detailed understanding of underlying plumbing systems either associated with stratigraphic carriers, seal bypass systems or a combination (Fig. 19b–i). In areas of structural complexity, seafloor geological mapping provides additional linkages between the spatial distribution of underlying structures, outcropping geology, and seafloor fluid flow features.

Seabed geochemical analysis revealed the presence of migrated thermogenic hydrocarbons including live oil and asphalts in the vicinity of extrusive mounds interpreted as mud or asphalt volcanoes, but also showed migrated hydrocarbons on exposed bedrock ridges with no obvious geomorphological features diagnostic of fluid venting. A relatively dense set of seabed geochemical samples helped to calibrate seismic scale fluid flow features, however, numerous fluid flow features have not been tested due to the geochemical survey being solely based on regional 2D seismic data (Fig. 19). This illustrates the importance of sampling density and site selection for which high resolution 3D seismic and remote sensing data can be used to prioritize piston core location over areas of thousands of square kilometres. In addition to the relevant selection of seep location, sampling density at a given location is also very important due to the dynamic evolution of seeps associated with episodic fluid flow and lateral migration of vents (Gay *et al.*, 2006).

Analysis of a relatively sparse set of SAR scenes with limited repeat coverage has shown the presence of 'third rank' and 'priority unassigned' slicks corresponding to oil slicks with an estimated 20–40% chance of being related to natural oil seepage. Integration with 3D seismic analysis and seabed geochemistry has helped to validate slick origins based on their co-occurrence with fluid expulsion features and near surface indication of migrated thermogenic hydrocarbon (Fig. 19j). Conversely, slicks have helped to refine seismic interpretation and reveal the presence of ambiguous seafloor features which might not have been interpreted as fluid flow features on a first-pass analysis (Fig. 19k).

Bottom-simulating reflection derived shallow geothermal gradients have highlighted the occurrence of thermal anomalies directly associated with highly conductive salt structure, as well as the possible effect of fluid advection along deep-rooted plumbing systems as suggested by the presence of distinct seep-related seafloor features including pockmarks, mud volcanoes and gas hydrate pingoes (Fig. 20).

Each of the techniques involved has its own advantages and limitations with 3D seismic data being continuous but relatively low resolution compared to discrete geochemical sample points. Specific discrepancies in our study include geochemically proven seafloor seeps with no geomorphological or sea surface characteristic diagnostic of seepage and some typical seismic fluid flow phenomena are uncalibrated by seabed geochemistry due to the discrete nature of these. However, the proposed iterative
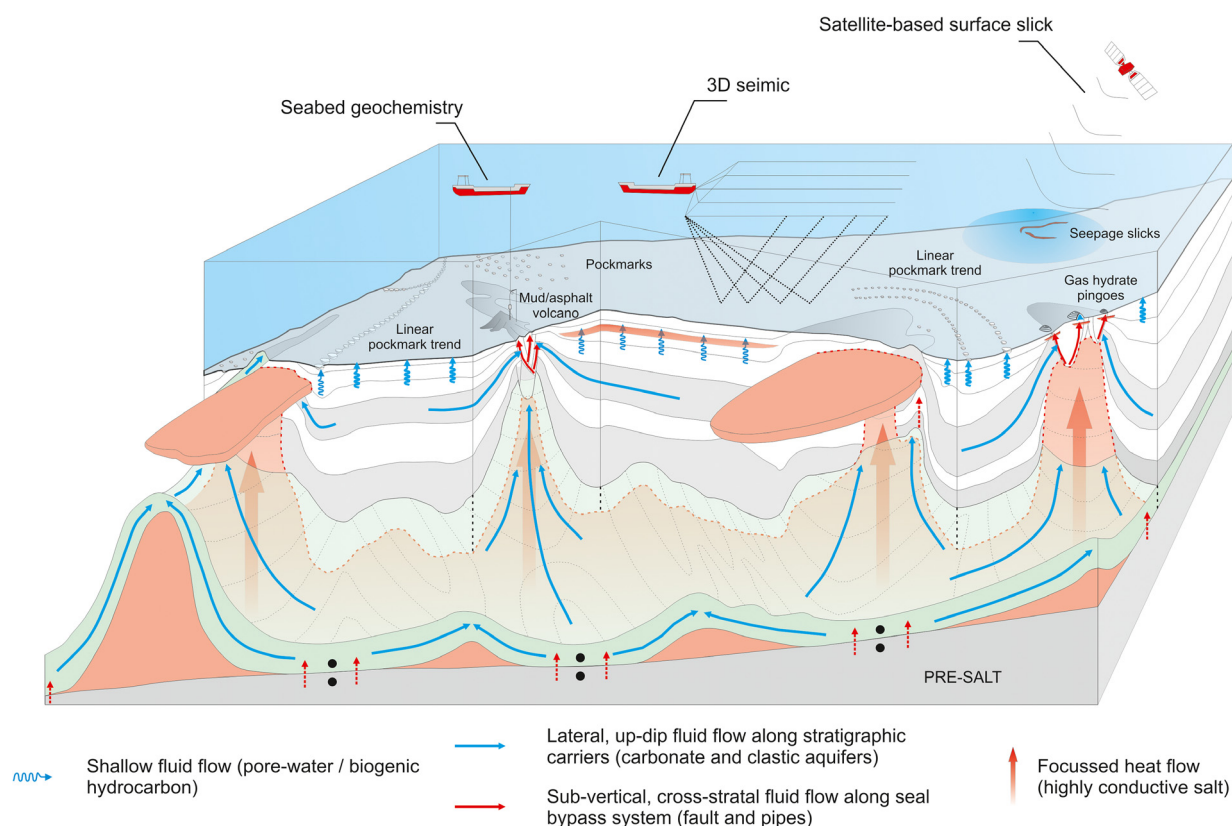

Fig. 20. Schematic 3D diagram synthesizing fluid flow phenomena and thermal regime within the study area with emphasis on the integration of multiple data set such as seismic, surface geochemistry and satellite seeps.

and integrated workflow highlights complementarities between each data set and offers a more nuanced and confident picture of the present-day fluid flow regime. In order to improve the analysis, access to deeper borehole data, higher definition, broadband, offset seismic volume, multi-azimuth 3D seismic data and electromagnetic data would be useful to further constrain the plumbing system and any non-aqueous fluid accumulations, as would a targeted seabed geochemical survey based on the 3D seismic mapping. Additional SAR scene interpretation combined with geochemical sampling at sea would help to improve slick confidence level, validate the occurrence of slicks associated with sustained oil seeps and constrain the origin of ambiguous seafloor features lacking ground truth geochemical data (Fig. 19l).

Fluid flow phenomena

Integrated analysis of remote sensing and geochemical data sets provides significant constraints to define the presence and intensity of past and present fluid flow as manifest by seeps and palaeo-seeps, fluid accumulations and seal bypass features. Surface slicks and seafloor fluid flow features represent the location and intensity of present-day seepage associated with distinct fluid migration processes. Widespread pockmarks within mini-basins are interpreted as the result of pore-water and biogenic gas migration derived from early sediment compaction and near-surface diagenesis of organic rich sediments (Bjørlykke, 1993; Horsfield & Rullkotter, 1994; Barry *et al.*, 2012). In contrast, pockmarks linked with deeper plumbing systems are often isolated and characterized by systematic distributions in relation to fluid migration paths (Ligtenberg, 2005; Gay *et al.*, 2007; Judd & Hovland, 2007; Andresen *et al.*, 2011). Palaeo-pockmarks are also inferred to have formed similarly, however, palaeo-pockmarks are not well documented through most sedimentary successions and are also relatively rare in our study area. The absence or limited occurrence of palaeo-pockmarks might in part be related to seismic imaging limitations, although modern 3D seismic data should allow pockmark detection at depths of several kilometres. Seismic mapping revealed that the lowest level at which palaeo-pockmarks are found in abundance corresponds to top Pliocene, with only few palaeo-pockmarks in the deeper sections. The high-quality of the 3D seismic volume provided high-confidence horizon interpretations at much deeper levels and the paucity of pockmarks in the deeper section is thus considered to be real, rather than an imaging artefact. The widespread occurrence of pockmarks within mini-basin at the top Pliocene and on the seafloor coincides with periods of deep-water pelagic sedimentation on a background of widely varying eustatic conditions due to glacial–interglacial fluctuations (Miller *et al.*, 2005). Such rapid changes in sea-level are associated with changes in hydrostatic pressure, and sea-level drops in particular may lead to repeated fluid expulsion from water and methane-rich sediments in the shallow subsurface

(Liu & Flemings, 2009; Hermanrud *et al.*, 2013). Additionally, the occurrence of extrusive mounds (mud/asphalt volcanoes) and gas hydrate pingoes, occasionally associated with near surface thermogenic hydrocarbons, surface slicks and overburden seismic anomalies, are directly linked to the presence of subsurface plumbing systems. Plumbing systems are either associated with stratigraphic carriers, seal bypass systems or a combination as a result of intense salt tectonics (Figs 19 and 20). Detailed mapping defines fluid migration pathways and highlights the relative importance of fluid flow along aquifers and/or through sealing sequences with the presence of seal bypass systems including faults and pipes. Specifically, mud or asphalt volcanoes are associated with aquifer/reservoir units (Albian shelf carbonates to Tertiary deep-water sands) buried by a few hundred metres of mud-prone strata on diapir crests while hydrate pingoes occur when flow units are cropping out at seafloor or covered by a few tens of metres of mud-prone strata. Allochthonous salt sheets generally disconnect their overburden from the deeper plumbing system and thus are generally only associated with seafloor seepage around their periphery or in areas that are still partly connected to adjacent minibasins as also found in other salt provinces (Andresen *et al.*, 2011; Shedd *et al.*, 2012; Figs 19 and 20).

Petroleum exploration

Integrated fluid flow studies provide an effective tool to address risk associated with hydrocarbon charge in frontier exploration settings and assess submarine geohazards during exploration and field development activities.

The presence of surface slicks and near-surface migrated thermogenic hydrocarbon in the vicinity of distinct extrusive mounds interpreted as mud or asphalt volcanoes, as well as on exposed bedrock ridges, provides strong evidence that an active petroleum system is present, as well as critical information on source, maturity, and migration pathways.

Geochemical analysis of near-surface migrated thermogenic hydrocarbons suggests a post-salt marine origin, however, possible contributions from pre-salt lacustrine source rocks cannot be eliminated. Further work using the full seismic volume and geochemical correlation between surface slicks, near-surface migrated thermogenic hydrocarbons, oils and source rocks will help to evaluate potential pre-salt oil migration into the post-salt interval across salt welds at the bottom of individual minibasins.

Migrated thermogenic hydrocarbons are associated with deep plumbing systems including stratigraphic carriers with permeable carbonate and clastic intervals, as well as seal bypass systems with faults and pipes over structural highs; however, change in geometries due to structural deformation associated with salt tectonics is a real issue to establish flow patterns at a given point in the past. Indeed, basin modelling calibrated to recent exploration

wells will help to constrain the relative timing and spatial relationships between source rock maturation, structural deformation of stratigraphic carriers, traps, distribution of seeps and palaeo-seeps, as well as the occurrence of seal bypass systems compromising the trap integrity of potential hydrocarbon accumulations.

Finally, fluid flow studies can help to determine the extent of geohazards and the mitigation needed for successful exploration and development activities (Heggland, 2004; Hadley *et al.*, 2008; McConnell *et al.*, 2012). The presence of steeply inclined and deeply buried flow units capped by mud/asphalt volcanoes suggests fluid pressures approaching the fracture gradient, in turn highlighting drilling hazards in the form of potential overburden flows, as well as the presence of gas hydrates for which increased heat flux along wells could induce hydrate dissociation and seafloor instability.

CONCLUSIONS

Integration of high-quality 3D seismic, seabed geochemistry and satellite-based imagery allows a comprehensive and complementary assessment of fluid flow phenomena associated with dewatering processes and hydrocarbon migration in the deep-water Kwanza Basin. Seismic scale fluid flow phenomena include pockmarks, mud or asphalt volcanoes, gas hydrate pingoes, as well as shallow subsurface features such as palaeo-pockmarks, direct hydrocarbon indicators (DHIs), bottom-simulating reflections (BSRs) and pipes.

Pockmarks and palaeo-pockmarks are widely developed in the salt minibasins and are mostly thought to be associated with dewatering and degassing of the shallow minibasin sediments, particularly during rapid sea-level drawdown during glacial–interglacial periods. Pockmarks directly linked with underlying plumbing systems tend to occur in the vicinity of salt-related structures and associated with hydrocarbon migration.

Extrusive mounds including mud or asphalt volcanoes and gas hydrate pingoes with associated BSRs are directly linked to deep plumbing systems comprising stratigraphic carriers and seal bypass systems. Elevated BSR-derived shallow geothermal gradients also show the possible effect of fluid advection around salt structures, in addition to thermal anomalies directly linked to highly conductive salt.

The presence of migrated thermogenic hydrocarbons including live oil and asphalt in the vicinity of extrusive mounds and on exposed bedrock ridges suggests the presence of an active petroleum system in the post-salt interval, with possible contribution from pre-salt source rocks.

The approaches outlined here are applicable and adaptable to any frontier exploration settings where data of different vintage and variable coverage are available. Further work on geochemical correlation between surface slick, seabed oil, oils and source rock, in addition to basin

modelling will help fine-tune our current understanding of fluid flow phenomena along continental margins with numerous applications, including petroleum exploration, submarine geohazards, marine ecosystems and climate change.

CONFLICT OF INTEREST

No conflict of interest declared.

REFERENCES

Abrams, M.A. (1992) Geophysical and geochemical evidence for subsurface hydrocarbon leakage in the Bering Sea. *Alaska Mar. Petrol. Geol.*, **9**(2), 208–221.

Abrams, M.A. (2005) Significance of hydrocarbon seepage relative to petroleum generation and entrapment. *Mar. Pet. Geol.*, **22**(4), 457–477.

Abrams, M.A. (2013) Best Practices for the Collection, Analysis, and Interpretation of Seabed Geochemical Samples To Evaluate Subsurface Hydrocarbon Generation and Entrapment.

Aharon, P., Roberts, H.H. & Snelling, R. (1992) Submarine venting of brines in the deep Gulf of Mexico: observations and geochemistry. *Geology*, **20**(6), 483–486.

Ala, M.A. & Selley, R.C. (1997), Chapter 8 The West African Coastal Basins. In: *Sedimentary Basins of the World* (Ed. by R.C. Selley), pp. 173–186, Elsevier, The Netherlands.

Alsop, G.I. (1996) Physical modelling of fold and fracture geometries associated with salt diapirism. *Geol. Soc. Lond. Spec. Publ.*, **100**(1), 227–241.

Andresen, K.J. & Huuse, M. (2011) 'Bulls-eye' pockmarks and polygonal faulting in the Lower Congo Basin: relative timing and implications for fluid expulsion during shallow burial. *Mar. Geol.*, **279**(1–4), 111–127.

Andresen, K.J., Huuse, M., Schødt, N.H., Clausen, L. & Seidler, L. (2011) Hydrocarbon plumbing systems of salt minibasins offshore Angola revealed by three-dimensional seismic analysis. *AAPG Bull.*, **95**(6), 1039–1065.

Anka, Z., Berndt, C. & Gay, A. (2012) Hydrocarbon leakage through focused fluid flow systems in continental margins. *Mar. Geol.*, **332–334**, 1–3.

Barry, M.A., Boudreau, B.P. & Johnson, B.D. (2012) Gas domes in soft cohesive sediments. *Geology*, **40**(4), 379–382.

BEGLINGER, S.E., DOUST, H. & CLOETINGH, S. (2012) Relating petroleum system and play development to basin evolution: west African South Atlantic basins. *Mar. Pet. Geol.*, **30**(1), 1–25.

BERNDT, C. (2005) Focused fluid flow in passive continental margins. *Philos. Trans. Roy. Soc. A Math. Phys. Eng. Sci.*, **363** (1837), 2855–2871.

BERNDT, C., BÜNZ, S., CLAYTON, T., MIENERT, J. & SAUNDERS, M. (2004) Seismic character of bottom simulating reflectors: examples from the mid-Norwegian margin. *Mar. Pet. Geol.*, **21**(6), 723–733.

BJØRLYKKE, K. (1993) Fluid flow in sedimentary basins. *Sed. Geol.*, **86**(1–2), 137–158.

BRICE, S.E., COCHRAN, M.D., PARDO, G. & EDWARDS, A.D. (1982), Tectonics and sedimentation of the South Atlantic rift sequences: Cabinda, Angola. In: *Studies in Continental Margin Geology* (Ed. by J.S. Watkins & C.L. Drake), pp. 5–18, American Association of Petroleum Geologists, Tulsa.

BROOKS, J.M., KENNICUTT, M.C. II, BARNARD, L.A., DENOUX, G.J. & CAREY, B.D. Jr (1983) Applications of Total Scanning Fluorescence to Exploration Geochemistry. pp. 393–400, Offshore Technology Conference.

BROWNFIELD, M.E. & CHARPENTIER, R.R. (2006) Geology and total petroleum systems of the West-Central Coastal Province (7203), West Africa. *Geol. Surv. Bull.*, **2207-B**, 52.

BURWOOD, R. (1999) Angola: source rock control for Lower Congo Coastal and Kwanza Basin petroleum systems. *Geol. Soc. Lond. Spec. Publ.*, **153**(1), 181–194.

CARTWRIGHT, J. (2007) The impact of 3D seismic data on the understanding of compaction, fluid flow and diagenesis in sedimentary basins. *J. Geol. Soc.*, **164**(5), 881–893.

CARTWRIGHT, J., HUUSE, M. & APLIN, A. (2007) Seal bypass systems. *AAPG Bull.*, **91**(8), 1141–1166.

COWLEY, R. & O'BRIEN, G.W. (2000) Identification and interpretation of leaking hydrocarbons using seismic data; a comparative montage of examples from the major fields in Australia's North West Shelf and Gippsland Basin. *APPEA J.*, **40**(1), 121–150.

DANFORTH, A. (1997), Petroleum systems of the Coastal Kwanza and Benguela Basins, Angola. In: *Hedberg AAPG/ABGP Joint Research Symposium "Petroleum Systems of the South Atlantic Margin"*, edited, November 16–19, 1997, Rio de Janeiro, Brazil.

DAVIES, J.H. (2013) Global map of solid Earth surface heat flow. *Geochem. Geophys. Geosyst.*, **14**(10), 4608–4622.

DICKENS, G.R. & QUINBY–HUNT, M.S. (1994) Methane hydrate stability in seawater. *Geophys. Res. Lett.*, **21** (19), 2115–2118.

DOOLEY, T.P., HUDEC, M.R. & JACKSON, M.P.A. (2012) The structure and evolution of sutures in allochthonous salt. *AAPG Bull.*, **96**(6), 1045–1070.

DUVAL, B., CRAMEZ, C. & JACKSON, M.P.A. (1992) Raft tectonics in the Kwanza Basin. *Angola Mar. Petrol. Geol.*, **9**(4), 389–404.

EVANS, R., STEWART, S. & DAVIES, R. (2007) Phase-reversed seabed reflections in seismic data: examples related to mud volcanoes from the South Caspian Sea. *Geo-Mar. Lett.*, **27** (2), 203–212.

GARCIA-PINEDA, O., MACDONALD, I., ZIMMER, B., SHEDD, B. & ROBERTS, H. (2010) Remote-sensing evaluation of geophysical anomaly sites in the outer continental slope, northern Gulf of Mexico. *Deep Sea Res. Part II*, **57**(21–23), 1859–1869.

GAY, A., LOPEZ, M., COCHONAT, P. & SERMONDADAZ, G. (2004) Polygonal faults-furrows system related to early stages of compaction – upper Miocene to recent sediments of the Lower Congo Basin. *Basin Res.*, **16**(1), 101–116.

GAY, A., LOPEZ, M., BERNDT, C. & SÉRANNE, M. (2007) Geological controls on focused fluid flow associated with seafloor seeps in the Lower Congo Basin. *Mar. Geol.*, **244**(1–4), 68–92.

GAY, A., LOPEZ, M., ONDREAS, H., CHARLOU, J.L., SERMONDADAZ, G. & COCHONAT, P. (2006) Seafloor Facies Related to Upward Methane Flux within a Giant Pockmark of the Lower Congo Basin. *Mar. Geol.*, **226**, 81–95.

GOLDHAMMER, R.K., COPE, M.J. & TUITJER, E. (2002), Cretaceous Sequence Stratigraphic and Paleogeographic Evolution of the Southern Kwanza Basin, Angola: Implications for Upper Cretaceous Siliciclastic Reservoirs (abs). in AAPG Annual Meeting, edited, March 10–13, 2002, Houston, Texas.

GREVEMEYER, I. & VILLINGER, H. (2001) Gas hydrate stability and the assessment of heat flow through continental margins. *Geophys. J. Int.*, **145**, 647–660.

GREVEMEYER, I., KOPF, A.J., FEKETE, N., KAUL, N., VILLINGER, H.W., HEESEMANN, M., WALLMANN, K., SPIEβ, V., GENNERICH, H.-H., MÜLLER, M. & WEINREBE, W. (2004) Fluid flow through active mud dome Mound Culebra offshore Nicoya Peninsula. *Costa Rica: Evidence Heat Flow Surv. Mar. Geol.*, **207**(1–4), 145–157.

GUIRAUD, R. & MAURIN, J.-C. (1992) Early cretaceous rifts of Western and Central Africa: an overview. *Tectonophysics*, **213** (1–2), 153–168.

HADLEY, C., PETERS, D., VAUGHAN, A. & BEAN, D. (2008) Gumusut-Kakap Project: Geohazard Characterisation and Impact on Field Development Plans, edited, International Petroleum Technology Conference.

HAQ, B.U., HARDENBOL, J. & VAIL, P.R. (1987) Chronology of fluctuating sea levels since the triassic. *Science*, **235**(4793), 1156–1167.

HARTWIG, A., DI PRIMIO, R., ANKA, Z. & HORSFIELD, B. (2012) Source rock characteristics and compositional kinetic models of Cretaceous organic rich black shales offshore southwestern Africa. *Org. Geochem.*, **51**, 17–34.

HAY, D.C. (2012), Stratigraphic Evolution of a Tortuous Corridor From The Stepped Slope of Angola. In: *Application of the Principles of Seismic Geomorphology to Continental-Slope and Base-of-Slope Systems: Case Studies From Seafloor and Near-Seafloor Analogues* (Ed. by B.E. Prather, M.E. Deptuck, D. Mohrig, B. Van Hoorn, and R.B. Wynn), pp. 163–180, SEPM (Society for Sedimentary Geology), Tulsa, OK.

HEGGLAND, R. (2004) Definition of geohazards in exploration 3-D seismic data using attributes and neural-network analysis. *AAPG Bull.*, **88**(6), 857–868.

HERMANRUD, C., VENSTAD, J., CARTWRIGHT, J., RENNAN, L., HERMANRUD, K. & NORDGÅRD BOLÅS, H. (2013) Consequences of water level drops for soft sediment deformation and vertical fluid leakage. *Math. Geosci.*, **45**(1), 1–30.

HO, S., CARTWRIGHT, J.A. & IMBERT, P. (2012) Vertical evolution of fluid venting structures in relation to gas flux, in the Neogene-Quaternary of the Lower Congo Basin. *Offshore Angola Mar. Geol.*, **332–334**, 40–55.

HOLDER, G.D., MALONE, R.D. & LAWSON, W.F. (1987) Effects of gas composition and geothermal properties on the thickness and depth of natural-gas-hydrate zones. *J. Petrol. Technol.*, **39** (9), 1147–1152.

Hood, K.C., Wenger, L., Gross, O. & Harrison, S. (2002), Hydrocarbon Systems Analysis of the Northern Gulf of Mexico: Delineation of Hydrocarbon Migration Pathways Using Seeps and Seismic Imaging. In: *Surface Exploration Case Histories: Applications of Geochemistry, Magnetics, and Remote Sensing* (Ed. by D. Schumacher & L.A. LeSchack), pp. 25–40. American Association of Petroleum Geologists and the Society of Exploration Geophysicists, Tulsa, OK.

Hornbach, M.J., Bangs, N.L. & Berndt, C. (2012) Detecting hydrate and fluid flow from bottom simulating reflector depth anomalies. *Geology*, 40(3), 227–230.

Horsfield, B. & Rullkotter, J. (1994), Diagenesis, catagenesis, and metagenisis of organic matter. In: *The Petroleum System – From Source to Trap* (Ed. by L.B. Magoon & W.G. Dow), pp. 189–199. American Association of Petroleum Geologists, Tulsa.

Hudec, M.R. & Jackson, M.P.A. (2004) Regional restoration across the Kwanza Basin, Angola: Salt tectonics triggered by repeated uplift of a metastable passive margin. *AAPG Bull.*, 88(7), 971–990.

Hudec, M.R. & Jackson, M.P.A. (2007) Terra infirma: Understanding salt tectonics. *Earth Sci. Rev.*, 82(1–2), 1–28.

Huuse, M., Jackson, C.A.L., Van Rensbergen, P., Davies, R.J., Flemings, P.B. & Dixon, R.J. (2010) Subsurface sediment remobilization and fluid flow in sedimentary basins: an overview. *Basin Res.*, 22(4), 342–360.

Imbert, P. & Ho, S. (2012) Seismic-scale funnel-shaped collapse features from the Paleocene-Eocene of the North West Shelf of Australia. *Mar. Geol.*, 332–334, 198–221.

Jackson, M.P.A., Hudec, M.R. & Hegarty, K.A. (2005) The great West African Tertiary coastal uplift: fact or fiction? A perspective from the Angolan divergent margin. *Tectonics*, 24 (6), TC6014.

Jones, D.O.B., Walls, A., Clare, M., Fiske, M.S., Weiland, R.J., O'Brien, R. & Touzel, D.F. (2014) Asphalt mounds and associated biota on the Angolan margin. *Deep Sea Res. Part I*, 94, 124–136.

Judd, A.G. & Hovland, M. (2007) *Seabed Fluid Flow: The Impact of Geology, Biology and the Marine Environment*. Cambridge University Press, Cambridge.

Karner, G.D. & Driscoll, N.W. (1999) Tectonic and stratigraphic development of the West African and eastern Brazilian Margins: insights from quantitative basin modelling. *Geol. Soc. Lond. Spec. Publ.*, 153(1), 11–40.

Katz, B.J. & Mello, M.R. (2000), Petroleum systems of the South Atlantic marginal basins-an overview. In: *Petroleum Systems of South Atlantic Margins* (Ed. by M.R. Mello & B.J. Katz), pp. 1–13. American Association of Petroleum Geologists, Tulsa, OK.

Kopf, A.J. (2002) Significance of mud volcanism. *Rev. Geophys.*, 40(2), 1005–1057.

Lawrence, G., Fleming, A., de Farago Botella, M. & Witt, T. (1998) Offshore Basin Screening: a viable commercial application of satellite radar to oil exploration, paper presented at Integrated Systems for Commercial Remote Sensing Applications (Ref. No. 1998/207), IEE Colloquium on Integrated Systems for Commercial Remote Sensing Applications 28 Apr 1998.

Ligtenberg, J.H. (2005) Detection of fluid migration pathways in seismic data: implications for fault seal analysis. *Basin Res.*, 17(1), 141–153.

Liu, X. & Flemings, P. (2009) Dynamic response of oceanic hydrates to sea level drop. *Geophys. Res. Lett.*, 36 (17), L17308.

Locarnini, R.A., Mishonov, A.V., Antonov, J.I., Boyer, T.P., Garcia, H.E., Baranova, O.K., Zweng, M.M. & Johnson, D.R. (2010) World Ocean Atlas 2009, Volume 1: Temperature. S. Levitus, Ed. NOAA Atlas NESDIS 68, U.S. Government Printing Office, Washington, D.C., 184 pp.

Logan, G.A., Jones, A.T., Kennard, J.M., Ryan, G.J. & Rollet, N. (2010) Australian offshore natural hydrocarbon seepage studies, a review and re-evaluation. *Mar. Pet. Geol.*, 27(1), 26–45.

Løseth, H., Gading, M. & Wensaas, L. (2009) Hydrocarbon leakage interpreted on seismic data. *Mar. Pet. Geol.*, 26(7), 1304–1319.

Lu, Z. & Sultan, N. (2008) Empirical expressions for gas hydrate stability law, its volume fraction and mass-density at temperatures 273.15 K to 290.15 K. *Geochem. J.*, 42(2), 163–175.

Lucazeau, F., Brigaud, F. & Bouroullec, J.L. (2004) High-resolution heat flow density in the lower Congo basin. *Geochem. Geophys. Geosyst.*, 5(3), Q03001.

Lunde, G., Aubert, K., Lauritzen, O. & Lorange, E. (1992), Tertiary uplift of the Kwanza Basin in Angola. In: *Géologie Africaine: Bulletin des Centres de Recherches Exploration-Production Elf-Aquitaine* (Ed. by R. Curnelle), pp. 99–117. Exploration-Production Elf-Aquitaine, Pau, France.

Lundin, E.R. (1992) Thin-skinned extensional tectonics on a salt detachment, northern Kwanza Basin. *Angola Mar. Petrol. Geol.*, 9(4), 405–411.

MacDonald, I.R., *et al.* (2004) Asphalt Volcanism and Chemosynthetic Life in the Campeche Knolls. *Gulf Mexico Sci.*, 304(5673), 999–1002.

Martin, V., Henry, P., Nouzé, H., Noble, M., Ashi, J. & Pascal, G. (2004) Erosion and sedimentation as processes controlling the BSR-derived heat flow on the Eastern Nankai margin. *Earth Planet. Sci. Lett.*, 222(1), 131–144.

Marton, L.G., Tari, G.C. & Lehmann, C.T. (2000), Evolution of the Angolan passive margin, West Africa, with emphasis on post-salt structural style. In: *Atlantic Rifts and Continental Margins* (Ed. by W. Mohriak & M. Talwani), pp. 129–149. AGU, Washington, DC.

Maslin, M., Owen, M., Betts, R., Day, S., Dunkley Jones, T. & Ridgwell, A. (2010) Gas hydrates: past and future geohazard? *Philos. Trans. Roy. Soc. A Math. Phys. Eng. Sci.*, 368 (1919), 2369–2393.

McConnell, D.R., Zhang, Z. & Boswell, R. (2012) Review of progress in evaluating gas hydrate drilling hazards. *Mar. Pet. Geol.*, 34(1), 209–223.

Milkov, A.V. & Sassen, R. (2002) Economic geology of offshore gas hydrate accumulations and provinces. *Mar. Pet. Geol.*, 19(1), 1–11.

Miller, K.G., Kominz, M.A., Browning, J.V., Wright, J.D., Mountain, G.S., Katz, M.E., Sugarman, P.J., Cramer, B.S., Christie-Blick, N. & Pekar, S.F. (2005) The phanerozoic record of global sea-level change. *Science*, 310(5752), 1293–1298.

Minshull, T.A. & Keddie, A. (2010) Measuring the geotherm with gas hydrate bottom-simulating reflectors: a novel approach using three-dimensional seismic data from the eastern Black Sea. *Terra Nova*, 22(2), 131–136.

Mitchum, R.M., Vail, P.R. & Sangree, J.B. (1977), Stratigraphic interpretation of seismic reflection patterns in depositional sequences, Part 6: Stratigraphic interpretation of

seismic reflection patterns in depositional sequences. In: *Seismic Stratigraphy–Application to Hydrocarbon Exploration* (Ed. by C.E. Payton), pp. 117–133. American Association of Petroleum Geologists, Tulsa, OK.

NAGIHARA, S., SCLATER, J.G., BECKLEY, L.M., BEHRENS, E.W. & LAWVER, L.A. (1992) High heat flow anomalies over salt structures on the texas continental slope, gulf of Mexico. *Geophys. Res. Lett.*, **19**, 1687–1690.

von NICOLAI, C. (2011), *The Interplay of Salt Movements and Regional Tectonics at the Passive Continental Margin of the South Atlantic, Kwanza Basin*. 143 pp, University of Potsdam, Potsdam.

O'BRIEN, G.W., LAWRENCE, G.M., WILLIAMS, A.K., GLENN, K., BARRETT, A.G., LECH, M., EDWARDS, D.S., COWLEY, R., BOREHAM, C.J. & SUMMONS, R.E. (2005) Yampi Shelf, Browse Basin, North-West Shelf, Australia: a test-bed for constraining hydrocarbon migration and seepage rates using combinations of 2D and 3D seismic data and multiple, independent remote sensing technologies. *Mar. Pet. Geol.*, **22**(4), 517–549.

PARTY, S.S. (1998) Site 1078, *In Wefer, G., Berger, W.H., Richter, C., Proc. ODP, Init. Repts.* **175**, 143–176.

PUFAHL, P.K., MASLIN, M.A., ANDERSON, L., BRÜCHERT, V., JANSEN, F., LIN, H., PEREZ, M. & VIDAL, L. (1998) Lithostratigraphic summary for Leg 175: Angola-Benguela upwelling system, *Proc. ODP. Init. Repts.*, **175**, 533–542.

QUIRK, D.G., SCHØDT, N., LASSEN, B., INGS, S.J., HSU, D., HIRSCH, K.K. & VON NICOLAI, C. (2012) Salt tectonics on passive margins: examples from Santos. *Campos Kwanza Basins Geol. Soc. Lond. Spec. Publ.*, **363**(1), 207–244.

ROBERTS, H.H. (2001), Fluid and gas expulsion on the northern Gulf of Mexico continental slope: Mud-prone to mineral-prone responses. In: *Natural gas Hydrates: Occurrence, Distribution and Detection* (Ed. by C.K. Paull & W.P. Dillon), pp. 145–161, Geophysical Monograph 124, AGU, Washington, DC.

ROBERTS, H.H., HARDAGE, B.A., SHEDD, W.W. & HUNT, J.J. (2006) Seafloor reflectivity—An important seismic property for interpreting fluid/gas expulsion geology and the presence of gas hydrate. *Lead. Edge*, **25**(5), 620–628.

SCHOLLNBERGER, E.M. (2001) Seismic sequence stratigraphy of the Lower Congo, Kwanza, and Benguela basins, offshore Angola, Africa, PhD thesis. Rice University, Houston, TX.

SERIÉ, C. (2013) Geophysical and geochemical characterization of fluid flow phenomena in the southern Kwanza Basin, offshore Angola: implications for petroleum systems analysis and hydrocarbon prospectivity in deep-water settings, PhD thesis. The University of Manchester, Manchester.

SERIÉ, C., HUUSE, M. & SCHØDT, N.H. (2012) Gas hydrate pingoes: deep seafloor evidence of focused fluid flow on continental margins. *Geology*, **40**(3), 207–210.

SHEDD, W., BOSWELL, R., FRYE, M., GODFRIAUX, P. & KRAMER, K. (2012) Occurrence and nature of "bottom simulating reflectors" in the northern Gulf of Mexico. *Mar. Pet. Geol.*, **34**(1), 31–40.

SHERIFF, R.E. (1985) Aspect of seismic resolution. In: *Seismic Stratigraphy II: An Integrated Approach to Hydrocarbon Exploration* (Ed. by O.R. Berg & D.G. Woolverton), pp. 1–10. American Association of Petroleum Geologists, Tulsa.

SHIPLEY, T.H., HOUSTON, M.H., BUFFLER, R.T., SHAUB, F.J., McMILLEN, K.J., LADD, J.W. & WORZEL, J.L. (1979) Seismic evidence for widespread possible gas hydrate horizons on continental slopes and rises. *AAPG Bull.*, **63**(12), 2204–2213.

SINGH, S.C., MINSHULL, T.A. & SPENCE, G.D. (1993) Velocity structure of a gas hydrate reflector. *Science*, **260**(5105), 204–207.

SLOAN, E.D. & KOH, C.A. (2008), *Clathrate hydrates of natural gases*.

SULTAN, N., COCHONAT, P., FOUCHER, J.P. & MIENERT, J. (2004) Effect of gas hydrates melting on seafloor slope instability. *Mar. Geol.*, **213**(1–4), 379–401.

UNCINI, G., BRANDAO, M. & GIOVANNELLI, A. (1998) Neocomian – Upper Aptian Pre-Salt Sequence of Southern Kwanza Basin: A Regional View (abs). In: *AAPG International Conference and Exhibition*, edited, November 8–11, 1998, Riode Janeiro, Brazil.

Van RENSBERGEN, P., HILLIS, R.R., MALTMAN, A.J. & MORLEY, C.K. (2003) Subsurface sediment mobilization: introduction. *Geol. Soc. Lond. Spec. Publ.*, **216**(1), 1–8.

Von HERZEN, R.P., HOSKINS, H. & Van ANDEL, T.H. (1972) Geophysical studies in the angola diapir field. *Geol. Soc. Am. Bull.*, **83**(7), 1901–1910.

WHITE, N., THOMPSON, M. & BARWISE, T. (2003) Understanding the thermal evolution of deep-water continental margins. *Nature*, **426**(6964), 334–343.

WILLIAMS, A. & LAWRENCE, G. (2002) The role of satellite seep detection in exploring the south atlantic's ultradeep water. In: *Surface Exploration Case Histories: Applications of Geochemistry, Magnetics, and Remote Sensing* (Ed. by D. Schumacher & L.A. LeSchack), pp. 327–344, AAPG Studies in Geology No. 48 and SEG Geophysical References Series No. 11.

YAMANO, M., UYEDA, S., AOKI, Y. & SHIPLEY, T.H. (1982) Estimates of heat flow derived from gas hydrates. *Geology*, **10**(7), 339–343.